# Mathematical Modeling of Immuno-radioprotector Delivery System Using a Monoclonal Antibody

By

Maha Alhassani

Thesis submitted to the

Faculty of Graduate and Postdoctoral Studies

In partial fulfillment of the requirements for the degree

Master of Applied Science in Biomedical Engineering

Ottawa-Carleton Institute for Biomedical Engineering

School of Information Technology and Engineering

University of Ottawa

Ottawa, Ontario, Canada

2015

# Abstract

Amifostine (WR-2721, delivered as Ethyol) is a radioprotector agent that reduces the likelihood of early and/or late biological effects by eliminating free radical particles during ionizing radiation fraction (radiotherapy). It activates in under normal tissues conditions to reduce mutation and fraction in DNA. Among 4000 prodrug compounds, amifostine is the only agent has been approved from the US Food and Drug Administration in clinical purposes. The main effective mechanisms of amifostine are based on scavenging for free radical, improving for DNA repair step and indication of cellular hypoxia. In the same time, this drug is not widely used around the world for different reasons mainly its high cost and toxicity level (lethal dose). Conjugating a monoclonal antibody with amifostine by a suitable linker is a process of Antibody Drug Conjugate producing *immuno-radioprotector* molecule hypothesis. Administrated molecule is an approach of targeted delivery therapy that increases the dosage uptake into particular area of treatment to minimize the dose distribution in non-targeted area in the body.

In the present work, we proposed a three-compartment system model to simulate the two-pore theory pathway of an *immuno-radioprotector* molecule when it is crossing the physiological barriers. The model investigated its distribution and elimination in porous media (with both large and small pores) within a pharmacokinetics compartmented model approach.

# Acknowledgements

First and foremost, I would like to express gratitude to my God “Allah”, the Almighty God for the blessing, kindness, and inspiration to be here today. Then, I would like to pass my thankful to our king Abdullah bin Abdul-Aziz who passed away after he inspired his great vision and leadership to us for a decade as king.

I would like to thank my advisor professor. Mustapha C.E. Yagoub for his full support, expert guidance, understanding and encouragement throughout my research. I also express my thanks to the examiners professor. Rony E. Amaya and professor. Khelifa Hettak, for their valued time and interests in my thesis.

I also, would like to express my thanks to Abdullah Aljanah and Gurpreet Gosal for their cooperation and helping me with their expertise.

Thank my parents, Talal and Hayat, for having faith in me and allowing me to be the ambitious person I am today. It was under their watchful eye that I gained so much drive and an ability to tackle challenges head on. And I am greatly indebted to my family grandmothers, siblings, and family members for their unconditional love and support from the distance. Finally, I would give my thanks to my friends in Canada who were with, to get me through the most difficult time.

Thank you Canada!

# Table of Contents

# List of Figures

# List of Tables

# List of Acronyms

| | |
|---|---|
| Ab | Antibody. |
| ADC | Antibody drug conjugate. |
| ADME | Administration, distribution, metabolism and elimination. |
| Ag | Antigen. |
| CEA | Carcinoembryonic antigen. |
| DNA | Deoxyribonucleic acid. |
| FDA | Food and drug administration. |
| HNC | Head and neck cancer, |
| IgG | Immunoglobulins G. |
| IM | Intramuscular administration. |
| IR | Ionizing radiation. |
| I.V. | Intravenous administration. |
| kDa | Kilo-Dalton. |
| LET | Linear energy transfer. |
| mAb | Monoclonal antibody. |
| ODE | Ordinary differential equation. |
| PC-linker | Photo-cleavable linker. |
| PK/PK | Pharmacokinetics/ Pharmacodynamics. |
| RBE | Relative biological effectiveness. |
| RNA | Reactive oxygen species. |
| ROS | Ribonucleic acid. |

| | |
|---|---|
| SC | Subcutaneous administration. |

## List of Symbols

| | |
|---|---|
| $T_\alpha \ and \ T_\beta$ | Alpha half-life and beta half-life (min). |
| Cpl | Molecular concentration in the plasma (nM). |
| $C_{i,O}^{B}$ | Bound antibody concentration in the intrestitium for each organ (O= t or l) (M=$\frac{ml}{min}$). |
| $C_{cop}$ | Concentration in each compartment (M=$\frac{ml}{min}$). |
| $C_{i,O}^{f}$ | Free antibody concentration in the intrestitium for each organ (O= t or l) (M=$\frac{ml}{min}$). |
| $C_i$ | Concentration in interstitial (M=$\frac{ml}{min}$). |
| $C_{pl}$ | Concentration in the plasma (M=$\frac{ml}{min}$). |
| $C_v$ | Antibody Concentration in the vascular space (M=$\frac{ml}{min}$) |
| $D$ | diffusion coefficient |
| $J_{solute}$ | Diffusion rate (ml/min). |
| $J_{volume}$ | Volumetric flow rate (ml/min). |
| $K_O^f$ | Association rate constant for the binding of antibody (/M. min). |
| $K_O^r$ | Dissociation rate constant for the binding of antibody (/min). |
| $K_a$ | Binding affinity constant for antibody ($M^{-1}$). |
| $K_{e,O}$ | Catabolic elimination rate for each organ (l or t) ($\frac{ml}{min}$). |
| $L_p$ | Constant of hydraulic conductivity ($\frac{Cm}{mm\ Hg.S}$). |
| $L_pS$ | Capillary hydraulic conductance. |
| $MW$ | Molecular weight (kDa). |

| | |
|---|---|
| $P$ | Vascular permeability factor ($\frac{cm}{s}$). |
| $PS_L$, $PS_s$ | Permeability surface area for large and small pores respectively (/min) |
| $P_c$ | Capillary hydrostatic pressure (mm Hg). |
| $Pe_{L,O}$, $Pe_{s,O}$ | Peclet number, the ratio of convection to diffusion across small and large pores. |
| $P_i$ | Interstitial hydrostatic pressure (mm Hg). |
| $R_O$ | Partition coefficient of antibody between vascular and extravascular space |
| $S$ | Surface area of transport exchanging ($cm^2$). |
| $W_t$ | Waiting time of concentration peak. |
| $\alpha_i$ | Fraction of hydraulic conductance attributed to pore type "$i$ ". |
| $\pi_c$ | Capillary protein osmotic (oncotic) pressure (mm Hg). |
| $\pi_i$ | Interstitial protein osmotic (oncotic) pressure (mm Hg). |
| $\sigma_{i,j}$ | Staverman's osmotic reflection coefficient (unit free). |
| $\Delta P_{i,j}$ | Transendothelial difference for solute "$j$" at pore type "$i$". |
| $\Delta\pi_j$ | Transendotheial osmotic pressure difference of solute "$j$". |

# Chapter 1. Introduction

Over the years, we have seen a rising need to treat tumour tissues and protect normal tissues during the treatment of cancer patients with radiation therapy and/or chemotherapy. This need has encouraged researchers from around the world to try and develop agents that could help. These protective agents are adjusted to work with radiotherapy as "radioprotectors" or with chemotherapy as "chemoprotectors". They were first conceived as a way to protect the armed forces against the use of nuclear weapons in World War II. In fact, numerous studies were conducted to produce various agents that could protect the soldiers during this war. The researchers found more than 4000 compounds as protectors, but the US **F**ood and **D**rug **A**dministration (FDA) has approved only one compound of radioprotectors, clinically known as Amifostine (WR-2721) [1].

In this thesis, we plan to investigate the use of this compound based on pharmacokinetics modeling and simulating. In fact, simulation is a promising area for researchers in drug development; it is considered a planning procedure and is thus regarded as the pre-stage of the experimental work. It is more convenient as well as less costly and time consuming for researchers to conduct a simulation rather than laboratory work. In this approach, we integrated two molecules and formulated mathematically the process based on physiological mechanism of the molecule bio-distribution in tissues.

## 1.1 Antibody Targeted Cancer Therapy:

An antibody (Ab) is a glycol-protein made up of amino acids and a small amount of carbohydrates. It has a large Y-shape (Y), which is used by the immune system in the

presence of a foreign substance in the body. At the cell's receptor, there is a substance of protein base that has a highly recognition with specific antibody known as antigen Ag (Δ). Each Ag has an epitope part (the specific piece of Ag that binds into an antibody) that can be in any substance that stimulates the immune system i.e. infection and diseases. In the cancer therapeutic, tumour cell surface has this epitope of Ag to interact with specific Ab's in the biological system. This antigen at the cell's surface is responsible for what goes in/out of the cells. Functionally, the treatment can be structurally manipulated in the research field to produce an antibody for each receptor antigen disease. Antibody engineering development is indeed one of the most promising areas in cancer therapy. Although the localization feature (affinity) of Ab can be used in delivery therapy, but at the same time, it is hard to obtain a useful antibody for clinical applications and to get it approved by the FDA [2].

There are five different classes of antibodies: IgM, IgD, IgG, IgA and IgE [2]. In this work, we used the IgG antibody to describe the general structural features of immunoglobulins. The IgG antibody is a large molecule with a molecular weight of 150 kDa, which runs as a delivery vehicle for drugs. It can be more localized and, consequently, minimize the dose of a certain drug, in this case Amifostine. Moreover, antibody-targeted molecule has three components, which are: the monoclonal antibody mAb (Y), the cytotoxic drug (in this thesis the Amifostine), and a linker (photo-cleavable linker) connecting the drug to the antibody (Y---Amifostine), see figure (1).

The therapeutic technique manipulates into a functional expression for each main part of the integrated molecule. First, based on the target receptor, mAb can be changed to attach it to the right antigen expression of tumour cells. Next, in targeted therapy, a

cytotoxic drug is usually used as a prodrug (anti-cancer) to kill tumour tissues after internalized the cell. We therefore followed the concept of targeting the cell by antibody while the conjugated drug (Amifostine) will act as protector for normal tissues. This conjugation can be accomplished when a suitable linker has the ability of chemically conjoining both sides with Amifostine and antibody. After attaching to its receptor, that linker (photo-cleavable linker) will release the drug into the environment. This releasing will distribute the drug and absorb it inside the normal tissue thus, activating the drug to make protection.

Locally, the linkage of mAb to this radioprotector (Amifostine) is a way of conferring to normal cells the power of protection and accelerating the cell reparation mechanism. It is used to create a higher level of protection from free radicals and to reduce the high toxicity dose of the radioprotector. The biological conjunction between a specific monoclonal antibody and Amifostine is called **A**ntibody–**D**rug **C**onjugates (ADC) [2]. To optimize the drug for protectors in radiotherapy, we have to re-evaluate the protection mechanism for this radioprotector. The protectors deliver a sufficient protection level to all cells around the targeted treatment area, except the malignant cells, without affecting the efficacy of the radio-treatment.

## 1.2 Problem Statement

The main objective of this thesis was to study the use of one of the most important prodrugs (i.e., Amifostine) for protection, while previously used for military purposes. Then, we investigated the use of ADC to overcome the limitation of this prodrug in radiotherapy as protector. Amifostine (WR-2721) is one of the most effective protection compounds. It has been reported that it is well tolerated in **H**ead and **N**eck **C**ancers

(HNC), whereas it had undesirable side effects with other cancers [3]. This caused certain dosage limitations and decreased the amount of the suggested drug to achieve the maximum level of protection. After conjugation, both molecules (Amifostine and antibody) will become as one agent molecule called "*immuno-radioprotector*" molecule. The molecule can reach the desire target and protect the normal tissues after breaking the linker by ionizing radiation and releasing Amifostine in the environment.

Since Amifostine is a toxicity prodrug, the problems of using Amifostine in radiotherapy are mainly related to the level of toxicity one can administrated (the dose based on a patient's weight) and its cost. Amifostine is generally well tolerated but its toxicity can cause some side effects as reported by FDA (i.e. hypotension, high emetogenic, emesis, nausea, fever) [3]. So there are numerous health issues to consider as well as the final cost of a therapy. Therefore, one can easily see the advantages of reducing the total dose of Amifostine. In fact, the treatment can be improved by antibody delivery associated with dual function of therapeutic gains. While radiation kills the tumours, Amifostine is protecting normal tissues from the side effects of radiation. However, financially speaking, because of the high cost of Amifostine, insurance companies limit its use in head and neck cancers, even if it helps patients overcome the healing time after radiotherapy.

Therefore, there is a need to simulate the pathway of the *immuno-radioprotector* molecule when it is crossing the physiological barriers, in order to investigate its distribution and elimination in predefined media. To achieve this purpose, the first step would be to collect reliable data. However, medical privacy and ethical rules have prevented obtaining data. On the other side, data available through the published

literature are based on too particular cases, and thus cannot be taken as generic. So, we first developed a pharmacokinetics model to serve as reference. This model, described in [4], was developed using a mathematical two-compartment configuration for antibody-targeted therapy of colorectal cancer. Once completed, we proposed a new model with a three-compartment configuration. Then, we made a comparative study to evaluate the concentration behaviour in each compartment of the system, for both the tumour and the liver models. The proposed model described the transportation of conjugated antibody with the Amifostine as *immuno-radioprotector* molecule (figure 1). It is an antibody-based therapeutic that has 28 approval drugs from the FDA for oncological purposes [5]. For all these agents, the releasing stage of drug in the biological system must be sufficient to kill the tumour in the desire area, whereas our agent (Amifostine) has a different mechanism and purpose in the biological system, i.e., to protect normal tissues that are surround the tumour. To the best of the author's knowledge, this is the first model investigating the use of Amifostine as conjugated drug with another molecule.

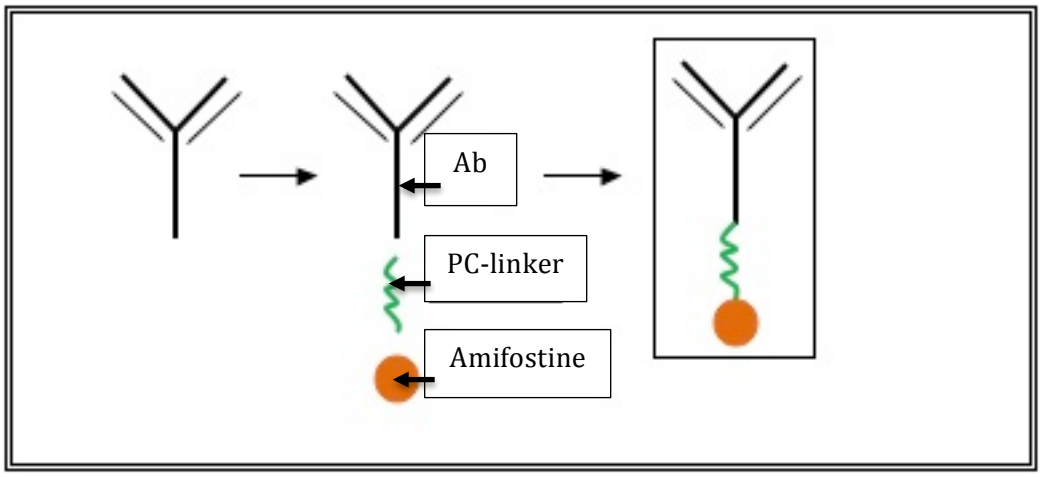


Figure 1: Immuno-radioprotector drug: describing the conjugated antibody with Amifostine using a photo-cleavable linker (PC linker) by (ADC).

To achieve this target, we studied the molecule according to a pharmacokinetic system. The model can describe the kinetic movements of molecule as macromolecule particle. It is based on mathematical equations (first order ordinary differential equations) considering the two-pore theory of macromolecular exchange crossing vascularity walls.

In this work, the *immuno-radioprotector* molecule was intravenously (i.v.) administered because we used the vascular space as an administrated space in the bloodstream. By using the specificity of antibody to the antigen and the selectivity of antibody to tumour, the molecule can reach the goal of reducing the total dose and the drug cost. Once the Amifostine will be absorbed by a normal tissue as WR-2721 (the inactive form), then the cytoprotective pathway will be ready to activate this WR-2721 into the activation form of protection WR-1065.

The general achievement of protection as pharmacokinetics system is following steps: i.v. administration (*immuno-radioprotector*), circulation in plasma, attachment to the antigen, releasing of Amifostine (the mechanism involves the selectivity between normal and malignant cells), the molecule will make the mechanism of transport across two-pore system, and Amifostine will be activated inside the normal cells to start the cytoprotective pathway, see figure 2.

The *immuno-radioprotector* molecule helps minimize the adverse effects of radiation on the normal tissues of patients during and after their radio-treatment. Targeted radioprotectors are expected to be more effective and less harmful to normal cells than the current treatment techniques, which entail the use of Amifostine along with radiotherapy.

## 1.3 Proposed Solutions and Contributions

A computational method was developed to model the two-pore theory. We first developed a two-compartment pharmacokinetics as described in [4], to serve as reference in our work. Next, we proposed a new model with a three-compartment configuration. Then, we made a comparative study to evaluate the concentration results in each tissue space of the system for two organ models: tumour and liver. To the best of the author's knowledge, this is the first model investigating the use of Amifostine as conjugated drug in targeted-therapy. Using the developed model, we then extracted the profile of plasma concentration (Cpl), the concentration profile and varied the initial concentration as a key parameter for the system to study its sensitivity on the model response.

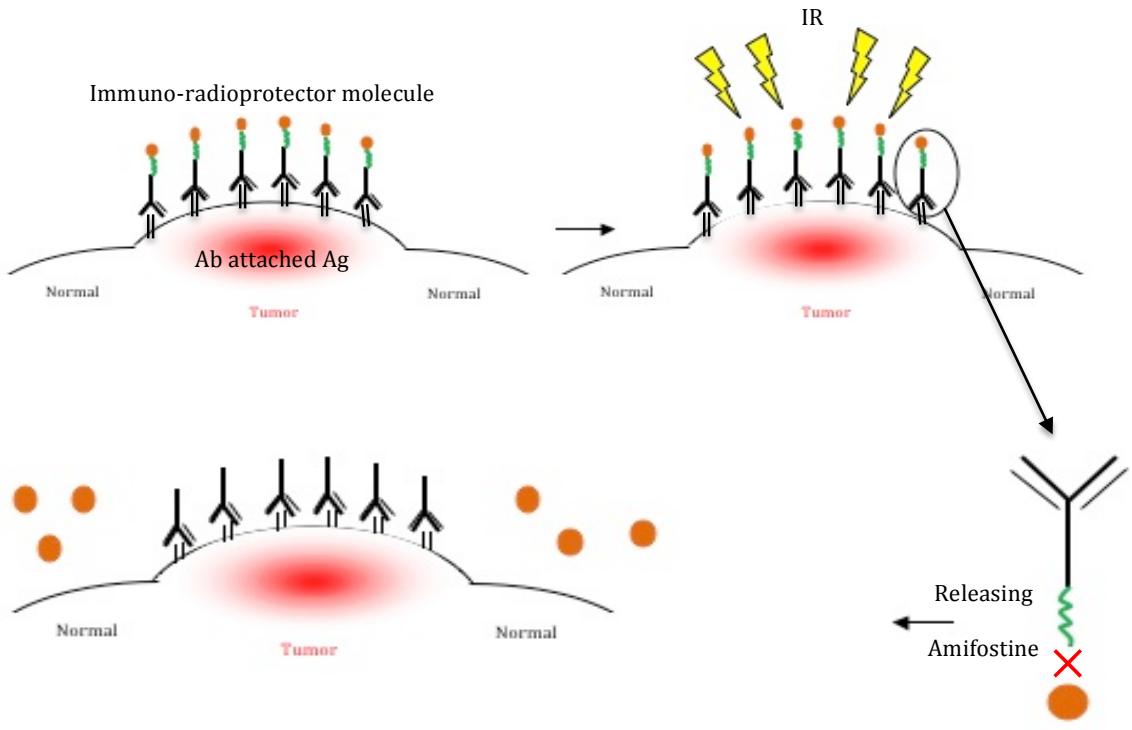


Figure 2: Hypothesis for the mechanism of the *immuno-radioprotector* molecule study.

The main reason for this work was to decrease the total dose of Amifostine needed (dose amount) to decrease toxicity and cost. Besides, it is going to increase Amifostine's presence in clinical proposals and in protection protocol regulations. A decreased dose of Amifostine per patient means that the insurance companies will be willing to cover more of the cost. Moreover, increasing the chance of using Amifostine in radiotherapy will be helpful for other several kinds of cancers and not exclusively for head and neck cancers (HNC) [6].

## 1.4 Document Overview

This thesis consists of six chapters. The first chapter introduces this research and provides the overview of the main concern of problem statement and the proposed solution. Chapter 2 gives background information and describes related that cover the topic from several fields of study. The mathematical theory behind our proposed methodology is the base of chapter 3. It depicts the state of the art relevant to the roles of macromolecules transportation in micro-walls. We therefore need to engineer the design and simulate the model, in order to use the data acquired to solve the problem. It details the mass transporters balance in each single compartment for the system and describes the lows and theories in pharmacokinetics study. Chapter 4 deals with the theoretical background required to develop our two models. The first model was setup to be used as reference in order to validate our results while the second model is indeed our main contribution. It can investigate the *immuno-radioprotector* molecule transportation phenomenon. Each model was derived for two organs (tumour and liver) knowing that each of them has specific formula in the form of first order differential equations (ODE). Chapter 5 shows the obtained results for each model as well as the comparative study

mentioned above. Chapter 6 concluded our work and summarize some of the directions that can be explored as future work to further improve our model.

# Chapter 2. Background and Literature Review

## 2.1 Radiation and Radiobiological Effects

Radiation can be in the form of waves or particles, and is generated from various sources. These sources of radiation include the radon found in houses, tainting from weapon testing locales, atomic accidents, and radiotherapy for tumours. Advances in the use of radiation are beneficial in the fields of prescription, industry and experimental examination. In this way, securing living frameworks away from the harming effects of radiation is critical in radiation science. It is likewise paramount in the radiotherapy of tumour patients, where normal tissues need to be protected while patients face ionizing radiation. There are two types of radiation: ionizing and non-ionizing. Non-ionizing radiation has less vitality than ionizing radiation; it doesn't have enough strength for excitation or ionization. Examples of non-ionizing radiation are visible light, infrared, radio waves, microwaves, and extremely low frequencies [7].

Ionizing radiation (IR) has a greater biological effect and higher level of risk than non-ionizing radiation, which is why the need to protect ourselves from these harmful effects is of utmost importance in the field of radiation, since 1896 [8]. Radiation is used in clinical (diagnostic or treatment) proposals as internal or external beam exposure. The ionizing radiation used in radiotherapy is essentially external-beams sent to patients. Conciliating treatment and protection is not that easy. Every patient under radiotherapy treatment receives a single or multi-field of ionizing radiation beams, depending on their case. Those beams have to be distributed based on a very high accuracy planning, in order to kill as many tumour cells as possible, in each radio-fraction. At the same time, it

has to protect the normal tissues (non-targeted tissues). The treatment can be a palliative fraction radiation for the whole body with no need for planned treatment. In therapy, protection means limiting radiation but not completely preventing it. In other words, the goal is not to avoid radiation but to use it safely. The exposure to ionizing radiation (IR) can make irreversible and detrimental changes in the cells. Accordingly, the interaction between ionizing radiation (IR) and biological cells can extract unstable and aggressive particles that cause damage at the cellular level. That radiation is capable of producing significant short and long-term biological effects in the event of exposure to human tissues [9].

When a human body receives photons (during x-ray or gamma ray exposure), it will interact with them. The absorption of radiation energy through biological material may lead to excite or ionize the atom or molecule. Excitation is the raising of an electron in an atom or molecule to a higher energy level without any ejection of electrons from its orbit. Ionizing energy, on the other hand, is the incident photon from radiation that has sufficient energy to overcome the binding energy and eject electrons from their orbits. There are different kinds of ionizing radiation: alpha radiation (α), beta radiation (β), neutron radiation (n), and photon radiation (gamma [γ] and X-ray radiation). The harming effects of ionizing radiation, which absorbs into the media, can be classified into two effects: direct and indirect. First, a direct effect of ionizing radiation (particulate radiation) occurs when a photon hits an electron in an atom or molecule, causing ionization. The electron now has sufficient energy to overwhelm the attractive force of the nucleus, which results in the ionization of an atom or molecule. It can directly produce chemical and biological changes in DNA. Theoretically, there are three

important processes occurring when photons interact with an object, for example the human body. These processes are the photoelectric effect, the Compton Effect, and pair production.

These processes can be distinguished based on the mass absorption characteristics of the target (the atomic number of the target, Z) and the energy of the incident photon. The radiobiological effects result from hitting the critical target in the biological cell. This is possible by interacting two different actions: direct interactions with DNA (ionizing or excited) in cells, and/or indirect actions that produce free radicals. Up to 60% of the human adult body is water, which means the body is mostly damaged due to biological molecules in a hydrous media. Therefore, radiation causes the formation of reactive oxygen species (ROS) with water particles in biological cells. Free radicals are ionizing atoms or molecule that are trying to stabilize by binding with outer electrons in another atom inside the biological media. This is processed as:

$$H_2O + \text{Radiation} \rightarrow H_2O^+ \text{ (ion radical)} + e^- \text{ (unpaired electron).}$$

$$H_2O^+ \rightarrow H^+ + OH^{\cdot}$$

$$e^- + H_2O \rightarrow H_2O^-$$

$$H_2O^- \rightarrow H^{\cdot} + OH^-$$

In the second step, the unpaired electron interacts with water $H_2O$ producing another free radical particle called the hydroxyl radical $^{\cdot}OH$. This particle possesses 9-electrons, of which only one is unpaired and has highly reactive free radicals, but the distance of reactive is short to hit DNA.

The final biological change is described simply as:

Incident ionizing radiation (photons) → Fast electron ($e^-$) → Ion radical → Free radical → Chemical changes from the breakage of bonds → Biologic effect [8].

At the DNA level, ionizing radiation interacts with matter and can possibly break DNA by hitting it with a direct interaction or an indirect interaction. The undirected interaction yields secondary electrons (free radicals) that interact with critical molecules introduced after the interaction with a first electron in an orbit atom. Photons, gamma and X-rays (uncharged) are classified as indirect ionization radiation, while electrons, positrons and alpha particles (charged particles) are directed ionization radiation because of their direct action with matter [8]. Harm refers to a break in the lesion position of DNA, based on which it can be classified into: single-strand breaks, double-strand breaks, and DNA–DNA and DNA–protein crosslinks. All these harms produced from ROS particles contain the most significant harmful particle, known as (OH). Damages affect DNA linkers and various exogenous with different positions in that DNA: same strand, opposite strand (inter-strand crosslink) and DNA-protein crosslink [10].

Radiosensitivity, LET, and RBE are three factors that affect cell survival and explain the degree of interaction with matter. The sensitivity level of each tissue differs depending on cell cycle, LET, cell type, dose rate, and oxygen concentration. Radiosensitivity is the probability that cells/organs will suffer from ionizing radiation per unit of dose, determined by the cell cycle [15]. Hence, the radiation is very aggressive when the cell is at the $G_2$-phase and the M-phase in the cell cycle. In contrast, the cell has a very high radioresistance when it is at the S-phase in the cell cycle as in figure 3 [11]

[8]. There is no clear answer yet to explain why such behavior studies observed a delay in the survival duration of cell lines when they were irradiated with various doses. They found that generally, the $G_2$-phase and the M-phase had taken about 2-4 hours to repair themselves, and that the DNA damage level was the main cause of this time delay [11].

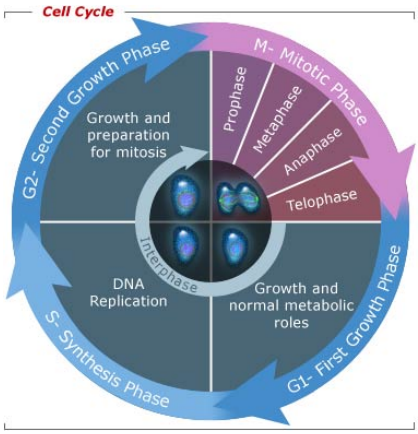


Figure 3: Cell cycle [11].

Further, radiosensitivity is high when the cell has a high ability of division, for instance in tumour cells, GI cells, and hematopoietic cells. On the other hand, it is very low if the cell has a long future division such as fetal cells and stem cells. They can also be unspecialized in nature (hematopoietic progenitor cells and stem cells - figure 4).

Generally, the relationship between the radiosensitivity of a tissue and its radiobiological degree is described inversely:

$$\text{Radiobiological effects} = \frac{1}{Radiosensitivity} \qquad \textbf{(1)}$$

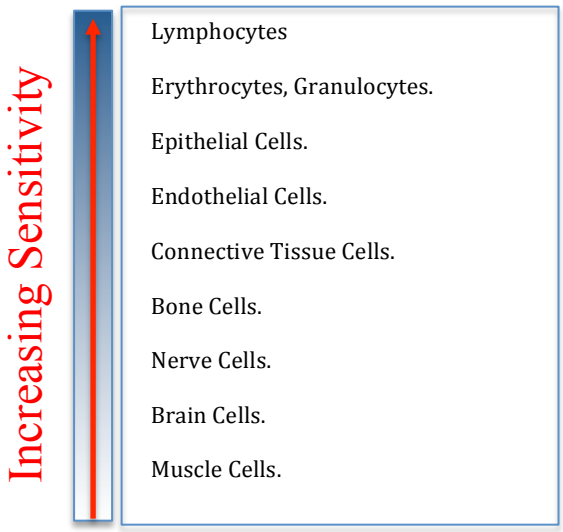


Figure 4: Radiosensitivity level in different organs/tissues.

A high Linear Energy Transfer (LET) is a quantity defined as the rate of energy transferred per unit distance expressed in (keV/$\mu$m), applied only to ionising charged particles that cause immediate harm [12] [8].

$$\text{LET} \propto \frac{mass}{speed} \qquad \textbf{(2)}$$

Optimal-LET is the optimised energy required to kill cells at a LET level between high and low. In other words, a high-LET is energy deposited over a short distance that overkills the cells, e.g., a high ionization density along the radiation track, such as alpha particles (≈80 keV/$\mu$m) (i.e. $\alpha, n \; and \; p$). A low-LET is an energy, generally sparse radiation, that causes damage to more than one track of the same cell, until cell death, such as the electron particle (≈0.2 keV/$\mu$m) (i.e. $\gamma, x, \sim \beta$)[13]. Low-LET is indirect as a form of ionizing radiation (electromagnetic -EM- radiation), i.e., it does not harm the cells directly but it can produce biological and chemical changes after absorption. When EM radiations give up their energy to be absorbed through a medium (atoms/molecules,

particles including water and macromolecules such as nucleic acids, lipids and proteins), they produce free radical charged particles [14]. A low-energy electron is generated by the ionizing events in the case of low Linear Energy Transfer (LET) radiation (uncharged particles) [8]. These free radicals, as defined previously, in turn cause damages at the cellular level of DNA. Another quantity related to LET is the Relative Biological Effectiveness RBE, which is the dose ratio and is generally independent of a LET that is less than 10 kV/$\mu$m (low-LET) reference, which gives the desired radiobiology to the one that it biologically affects [15].

## 2.2 Radioprotector Agents

For many years, scientists have been trying different methods to treat cancer patients who are receiving a high IR dose without harming the normal tissues. IR produces extra unpaired particles called free radicals in irradiated cells. These particles are chemically highly reactive with other tissues once the IR is absorbed in the target treatment area. Moreover, there exist several techniques that, combined together in different ways, can eliminate the radiobiological effects without reducing the treatment dose. The most remarkable group of true radioprotectors is the sulfhydryl compound containing a natural amino acid cysteine. Latarjet and Ephrati described in 1948 the chemical structure of radioprotector molecules $HO_2CCH$ ($NH_2$) CH2SH. At the same time, researchers discovered the cysteamine protector SH-$CH_2$-$CH_2$-$NH_2$ [8]. To describe the effectiveness of a radioprotector, one can use the dose-reduction factor DRF [16]. The structural features of these compounds are a free -SH group at the end of the molecule, a strong binding function of amine -$NH_2$ or guanidine at the other end of structure, and a straight chain of two or three carbon atoms in between. The SH group is the most active

part in cytoprotection. First, it works to scavenge free radicals which are damaging DNA. Second, the hydrogen atom helps repair the DNA's damage [17].

Radioprotectants are one of the three main classes of radiation countermeasures, along with radiation mitigators and therapeutic agents [17]. The difference between radioprotector agents and radiation mitigators is the time at which it is taken: before the treatment, during the treatment, or after the treatment, respectively. The first two classes work as protection agents in radiotherapy [18], while the third class –therapeutic agents- can be used before and/or after the fraction of radio-treatment for each patient [19].

Radioprotectors can reduce most of the unwanted side effects and provide very good protection from ionizing radiation, for the majority of the organs. Moreover, these cytotoxic agents have to be tolerated and have an acceptable toxicity level. Radioprotectors can be administrated through oral, intramuscular, intravenous or subcutaneous methods [17]. The first main cytoprotector agent approved for protection from free radicals is Cysteine, while the only approved active aminothiol agent is Amifostine WR-2721. Since 1969, the latter appears to be the best radioprotector for use in radiotherapy. Up to now, WR-2721 is the only drug approved by the FAD for clinical use in hospitals [17]. This active metabolite penetrates through the cells until it is dephosphorylated by the enzyme alkaline phosphatase with a higher pH compared to the hypoxic tumour tissue. Furthermore, this enzyme, present in the human lung cells, is 275-fold higher than in other "non-small cell" lung cancer cells, exists in very high levels in capillaries, and is barely present, with low activity, in many tumours [20]. Alkaline phosphates regularly requires an alkaline environment for an enzymatic activity [21]. Amifostine selectivity can meet these requirements and stimulate the activity of alkaline

phosphatase. Alkaline phosphatase exists in most tissues but the environmental differences between normal tissues and tumour tissues has an effect on the selectivity [22] [21]. The clinical use of WR-2721 can therefore protect normal and tumour tissues and increase the overall therapeutic gain.

### 2.2.1 Chemical and Biological Structure of Amifostine

Amifostine is classified as a macromolecule particle that has the purposeful function of circulating through blood flow and the capillary system to reach tissues under specific conditions. Structurally, Amifostine (Ethyol) is an organic thiophosphate prodrug with a molecular weight of 214.224 g/mol (Da). N-terminal is the right side of conjugation in Amifostine. It is part of a secondary Amin group ($-NH_2$) because it is more reactive than the primary nucleophile Amin group in the chemical structure figure 5.

In vivo, alkaline phosphatase activates the cytoprotective thiol metabolite to WR-1065 form. The most interesting part in the chemical structure of Amifostine is the aminothiol group that has the thiol group (-SH) to scavenge free radicals. Furthermore, WR-1065 (the active form of Amifostine) is involved in another metabolized process (oxidation) to produce disulfide molecules (WR-33278) to act as an additional protection, Figure 6 [23]. The limitation of accessibility to all normal tissues is the high bioavailability, except in the central nervous system because of the barrier of the brain, which prevents the brain from the macromolecule particle sizes [17]. The molecular structures of Amifostine (WR-2721) are $C_5H_{15}N_2O_3PS$ = $H_2N$-$(CH_2)_3$-NH-$(CH_2)_2$-S-$PO_3H_2$; Molecular weight (Mw) = 214.2 Da and (WR-1065) $C_5H_{14}N_2S$ = $H_2N$-$(CH_2)_3$-NH-$(CH_2)_2$-SH; Molecular weight (Mw) = 134.3 Da, respectively [24].

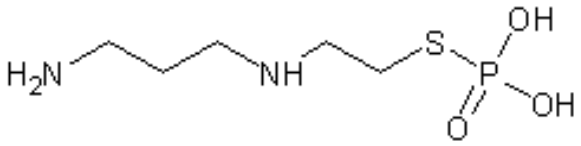


Figure 5: Chemical structure of Amifostine (S-{2-[(3-Aminopropyl) amino] ethyl} dihydrogen phosphorothioate)

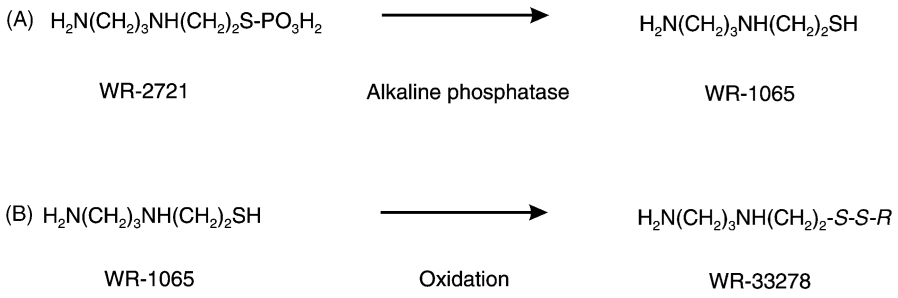


Figure 6: Metabolism of Amifostine- (A) dephosphoration and activation of WR-2721, (B) Oxidation step of additional protection [4].

Macromolecules (macro = large) are large molecules that have a particular mechanical mode of transportation in plasma, in order to reach the body cells. There are four main kinds of particles in the biological system: proteins (with which we are concerned in this study since these particles provide different functions such as support, storage, transportation, cell communication, movement, and defense), lipids, carbohydrates, and nucleic acids (DNA and RNA).

## 2.3 Pharmacokinetics

Pharmacokinetics (PK) allows us to study the medications and their pharmaceutical behaviours as mathematical equations. These equations describe and predict the pathways of the drug in the physiological system. It is a technique focused on the total plasma concentration of any organ in the body in order to evaluate: Absorption,

Distribution, Metabolism and Excretion “Elimination” (ADME). ADME describes the clearance from the blood in respective the time period of clearance. Dr. Bagshawe proposed such pharmacokinetic methodology over two decades ago [25] [26]. A principal understanding of the physiological path is then required to outline a suitable medication regimen for a patient.

### 2.3.1 Amifostine Pharmacokinetics

Cytoprotection reduces the early radiobiological effects (e.g. myelotoxicity, immunologic toxicity, radiation mucositis, neurotoxicity, cardiac and pulmonary toxicity, and skin toxicity) as well as the acute radiobiology of ionizing radiation (e.g. skin, muscle, breast, or lung fibrosis, xerostomia, necrosis of bone and soft tissues) [17]. It can also reduce the stochastic effects such as leukemogenesis and tumourigenesis. The pharmacology of Amifostine halts the development of a neoplasm by enhancing this effect of the radiation [17]. Amifostine has been studied as pharmacokinetics frame from its administration to its elimination as a summation of two exponential clearance decays of the drug from the body. The first is a rapid cleared initial phase from the plasma ($\alpha$), with very high values of 258 and 126 L/h when the doses are equal to 740 or 910 mg/m$^2$, respectively [20]. Then, we have a slower second phase called ($\beta$). Intravenously, 90% of the Amifostine disappears from the plasma 6 minutes after its administration, (table 2-1) [27].

Absorption is the first stage of Amifostine pharmacology that was administrated intravenously (i.v.), because of its compliance and efficiency compared to a subcutaneous administration (SC) [28], but also because it is more concentrated than other types of administration in blood and/or plasma (as a radiolabeled compound) [29].

Table 2-1: Pharmacokinetics data tested and published to identify Amifostine.

| | General pharmacokinetic data |
|---|---|
| **Bioavailability** | Complete availability [17] |
| **Clearance from the plasma** | $t_{1/2}$ ($\propto$) ≈ 0.88 minutes [31] |
| **Elimination** | $t_{1/2}$ (β) = 8.8 minutes [31] |
| **Maximum tolerated dose (MTD)** | 740 or 910 mg/m$^2$ (intravenous dose) [17] |

Oral administration is not an option because it is first difficult to use in cancer therapy and also due to the fact that Amifostine has poor oral efficiency because of the polarity of the drug's structure and the hydrolyzed feature in acidic media. Polarity creates a boundary to prevent the drug from crossing the lipoid membranes [29].

The bio-distribution of Amifostine characterizes the second stage of pharmacology; it starts 15 min. after administration, and reaches the maximum peak of distribution after 30-60 min. [29]. Indeed, Amifostine is distributed in the normal tissues of each organ that have an altered level of absorption, from the highest to the lowest. The highest level was found in the kidneys and the submandibular salivary gland, with substantial levels in the liver, the gut, and the lung. In contrast, the lowest level was found in the skin and the brain. The brain's barrier is its main protection against the penetration of macromolecule particles [17] [29].

Amifostine can activate the metabolism when it is dephosphorylated to the free thiol by the microenvironment of normal tissues; whereas tumour tissue is not expected to attenuate Amifostine through the surface of a tumour cell [24] because the medium does not often have a high pH (tumours are more acidic than normal tissues) [30]. For a pH environment, Amifostine protects normal tissues because it exists in normal tissues (100-fold greater concentration) [31]. The mechanism of action is structurally based on two steps of metabolisms. The first metabolic step of WR-2721 is the free thiol metabolite "dephosphorylation", which becomes WR-1065 by the membrane-bound enzyme alkaline phosphatase rapidly after taken it up into the cells [20]. It works as a first responsible line of protection to scavenge the free radical, donate hydrogen ions to free radicals, use oxygen and directly bind and inactivate cytotoxic drugs in the targeted area. The concentration of the drug in the normal tissues is higher than the concentration in tumour tissues, as vascularization is usually more prominent in normal tissues than in tumours. Thus, cytoprotective effects are largely limited to normal tissues [20]. The second step is when WR-1027 can be further oxidized to the form of disulfides WR-33278 (symmetrical plus mixed disulfide) [20] [32].

In the elimination stage, Amifostine and its activated metabolism forms are rapidly cleared from the plasma and excreted in the urine. WR-1065 has much slower clearance than Amifostine, with a half-life of 13.6 hours. Multiple doses could help increase the peak level of WR-2721 and disulfides [32].

### 2.3.2 Monoclonal Antibody Pharmacokinetics

The concept of monoclonal antibodies (mAbs) as pharmaco-therapeutic agents began in the mid-1980s. Their development was clinically approved as mAb muromonab-

CD3 to prevent acute organ rejection [33]. Over the past 30 years, therapeutic mAbs have become an increasingly important component of pharmacotherapy and have made a significant impact on the drug discovery and development process. It is estimated that more than 500 mAbs are presently in development and that the U.S. FDA is currently approving approximately 30 mAbs under Biologic License Applications [33].

For more than 20 years, cancer treatments have involved several methods that have a high accuracy of delivery and low toxicity. Many antibody models have been proven to have non-linear Pharmacokinetic (PK) profiles. Specifically, the first mAb PK compartmental model, published in 1971, was designed to represent different tissues and organs as a way to study the physiological processes (e.g. blood flow, lymph flow) [34]. Moreover, the study of PK has had other challenges related to specific physiological processes such as the capillary fluid exchange, the interstitial fluid, and lymph flow via convection and diffusion forces. The two-pore model is a typical model that can overcome those challenges in a system that can describe and provide the behaviour of any drug as a function of time. It has been designed for the pharmacokinetics of macromolecules, e.g., therapeutic proteins like mAb.

Antibodies can be administrated into the body by intravascular (intravenous i.v.) or extravascular (subcutaneous SC, intramuscular IM) means, based on a systemic absorption target. Oral administration is limited, as discussed above [35]. Antibodies are rapidly distributed in the plasma but have slow exchanges with the extracellular space. Furthermore, antibody is a hydrophilic drug unlike other small molecules that can diffuse the intravascular space directly. For that reason, it transports convection and absorbs through the lymphatic vessels into the blood. Also, antibodies can diffuse and cross the

blood vessels to distribute antibodies into a specific area of the injected target. The bioavailability of antibodies after reaching the maximum range of plasma concentration is reported to be between 50 and 100%, (table 2-2) [35] [36].

Table 2-2: General pharmacokinetic data of monoclonal antibody.

| | General Pharmacokinetic Data |
|---|---|
| **Bioavailability** | Generally is 50 and 100% [35] |
| **Elimination** | $t_{\beta}$= 86.92 hours [39] |
| **Clearance** | $t_{\propto} \approx$ 12.74 hours [39] |

Antibody distribution has been modeled using the physiological laws of macromolecule exchange, which mainly include convection, diffusion and several other processes such as transcytosis, binding, and catabolism at the binding site [37]. The distribution of the antibody penetration into a medium is fundamentally determined by the rate of administration of the i.v. infusion of the molecule into the extravascular space, the rate of distribution within the tissue, the rate of antibody binding, and the rate of elimination from the tissue [35]. Because of its large size compared to other molecules, mAb transports fluid from the blood to the interstitial fluids of tissue via a very slow process, therefore being seen as diffusion rather than a convection process. Furthermore, the net flow is determined by the equivalent quantification of the filtration, the reflection of antibodies in the tissues, and the permeability of the antibody [38].

The elimination of most small-molecule drugs is typically done through filtration into urine, secretion into bile, and biotransformation (metabolism or catabolism). In the kidney, the elimination is primarily a mechanism of clearance but it is also eligible to be a mechanism for IgG antibodies and large molecules. The same is true with secretion, which prevents the clearance of IgG antibodies but is taken into intracellular catabolism. [37].

## 2.4 *Immuno-Radioprotector* Molecule: Mathematical Modeling

Based on the above, several immuno-radioprotector molecule models have been developed for therapeutic and diagnostic purposes. Antibodies have fragments that can also be used in the same kind of research but we focused on the main monoclonal antibody, IgG. Any antibody has to pass all trial stages (I, II and III clinical trials) for it to be selected as an appropriate molecule candidate. These selections are meant to develop this antibody in order for it to be approved by the FDA after trial stage (i.v.). Under these conditions, the development and simulation of pharmacokinetics models can be seen as the fundamental blocs of drug development.

Mathematically, the *immuno-radioprotector* model is a pharmacokinetics of molecules in terms of a two-compartment model representing a model consistent with a peripheral compartment and a central compartment. Each compartment has a dependent parameter equation that describes the rate of change of bio-distribution in full systemic compartments (the mass balance). In the PK cancer model, the molecule administrates in a vascular space (blood/plasma), which is a central compartment of the system as a first-

order kinetics process. The molecule is then concentrated in the peripheral compartment, which is the target tissue (tumour and normal tissues in our case) [40].

## 2.5 Conclusion

In this chapter, we exposed the biological phenomena involved in cancer treatments. The next step will be to set-up the mathematical equations that model the movement of the drug from its administration to its elimination. Therefore, the next chapter will be devoted to the mathematical theory behind macromolecule transportation.

# Chapter 3. Mathematical Theory of Macromolecule Transportation

## 3.1 Fluid Transportation:

The transportation of molecules has various requirements. These are a combination of vascular space, interstitial space, and lymphatic space distributed within the space [41]. The transportation of macromolecules crosses three main bio-physiological barriers (microvascular walls): a heterogeneous blood supply, elevated interstitial pressure, and large transportation distances in the interstitium, Figure 7. All these barriers are governed by the localization of the macromolecules in the tumour [42].

There are different paths to take to cross these entire barriers and enter the tumour circulation in order to reach the target. Each particle or molecule could move via vascular space by distribution, crossing the microvascular wall and entering the interstitial space.

Transportation is regulated by the roles of the macromolecules that are exchanged between the spaces. They are standardized according to a convection and diffusion process in the capillaries [42]. These vascularity walls in the capillaries have a layer of thick cells called the endothelial cells [43].

### 3.1.1 Theoretical Background of Solute Transportation:

The theoretical background of solute transportation as a flux function on time (mol/min) can be described by the convection-diffusion equation (solute flux):

$$J_{Solute} = J_{diffusion} + J_{convection}$$

$$= \text{Fick's Law } (\frac{\text{mol}}{\text{min}}) + [\text{ Effective volume flux } (\frac{\text{ml}}{\text{min}}) . \text{Concentration } (\frac{\text{mol}}{\text{ml}})] \quad (3)$$

This equation describes the full system for transportation part for any macromolecule. It is basically based on the two main theories. First, the Ficks's law, which deals with the two way directions of movement. Second, the effective one direction volume transportation through the pores based on pressure forces in each space and the molecular concentration as a part of effective parameters in molecular exchange.

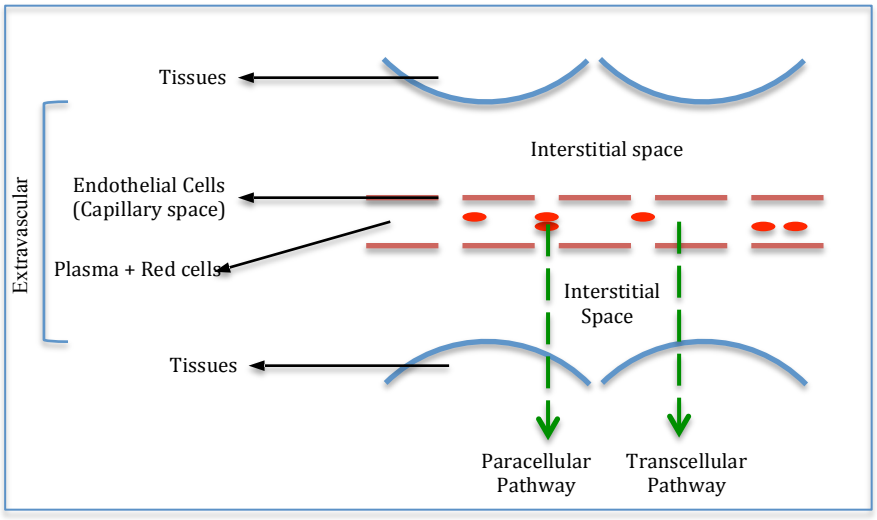


Figure 7: Diffusion and filtration of fluid molecules between the capillary and the interstitial fluid space.

1. Fick's Law of diffusion and selectivity

The movement of solutes through the barrier is a passive diffusion that depends on the concentration gradient and has no need for transportation energy (i.e. ATP energy). Fick's law describes the differential rates of molecule movement through the membrane (exchanges across membranes) from one site to another, and explains the physical process of osmosis. When the diffusion transportation of solutes happens in the direction of the concentration gradient (from high to low), it will continue until the concentration differential is in equilibrium.

Crossing the membrane depends on certain factors: surface area (A), the thickness of the membrane or "movement distance" (X), and the difference in the concentration gradient (C). It is given as a flux density or diffusion date of solute [44]:

$$J_{solute} = -D\,A\,\frac{dc}{dx} \qquad \textbf{(4)}$$

where D is the diffusion coefficient, replaced here by the permeability coefficient of the membrane in a biological system. It is related to the size of molecule (molecular weight MW) and the polarity of the solute as

$$D = \frac{permeability}{\sqrt{MW}} \qquad \textbf{(5)}$$

The concentration gradient is replaced by the difference in concentration on either side of the membrane. Thus,

$$J_{solute} = -D\,A\,\frac{dc}{dx} + (J_{volume}\,.\,C) \qquad \textbf{(6)}$$

2. Volume flow rate (Starling's equation):

In normal conditions, the partition of fluid acts under four pressures (forces): capillary hydrostatic pressure $P_c$, interstitial hydrostatic pressure $P_i$, capillary protein osmotic (oncotic) pressure $\pi_c$, and interstitial protein osmotic (oncotic) pressure $\pi_i$. These forces move the fluids in and out of the capillaries. Filtration movement occurs when the fluid leaves the capillary by a pushing force of ($P_c > \pi_c$), which means that any positive force works on transporting the fluid from inside the capillary toward the interstitial space [43]. In this condition, filtration and flow lymph increase based on the increase of $P_c$ [45]. Ultrafiltration or reflection movement occurs when fluid enters (absorption) the capillary by a pulling force of ($P_c < \pi_c$), which means that any negative force affects the movement in the reverse direction of transportation. In a steady state, the mechanism of transcapillary fluid helps the proteins flow from the plasma and cross the micro wall by a filtration force [45]. The accumulation of plasma portions in interstitial space will then directly disturb the equilibrium in the media on both sides of the wall. By this force, the medium will start returning to its balance by a volume redistribution of plasma portions among the spaces [45]. A homoporous membrane is under the effect of these four forces. Thus, the equilibrium between two direction exchange (filtration and reflection) at both sides of the micro-wall can be expressed as

$$J_{volume} = (filtration + reflection) \quad \textbf{(7)}$$

Mathematically, in case of homoporous membrane the rate of the flux movement of fluids in vascular ($J_v$), or the volume flow rate, is governed by a convection force and is proportional to the leakage of fluid from the vascular space. In turn, it is proportional to two differences in pressures: (1) the difference between the vascular and the interstitial

hydrostatic pressure $\Delta P$ (mm Hg), and (2) the difference between the vascular and interstitial osmotic pressure $\Delta\pi$ (mm Hg), which is characterized by a constant known as the osmotic coefficient reflection σ [42]. It is close to 1 in macromolecule transportation and close to zero in the case of a small molecule. The equation is then given as:

$$J_{volume} = [(P_c - P_i) - \sigma (\pi_c - \pi_i)] \quad \textbf{(8)}$$

3. Concentration

Convection only has one direction of movement (vascular to interstitium). It is related to the fluid leakage from vascular space $J_{convection}$ $\left(\frac{ml}{min}\right)$ [42]. In contrast, diffusion can move in either direction (vascular to interstitium or interstitium to vascular). This means that diffusion is proportional to the surface area S ($cm^2$) of transportation and to the difference in concentration ($\Delta C = C_{pl} - C_i$) ($\frac{ml}{min}$) for both sides of the microvascular wall [42]. The concentration is referred to as the vascular permeability factor P ($\frac{cm}{s}$) and the constant of hydraulic conductivity $L_p$($\frac{Cm}{mm\ Hg.S}$) of endothelium cell barrier is described by the modern version of Starling's equation [44]. The full set of equations used to explain the transportation of macromolecule solute can be given as:

$$J_{solute} = -D\ A\ \frac{dc}{dx} + (J_{volume}\ .\ Concentration) \quad \textbf{(9)}$$

$$J_s = -D\ A\ \frac{dc}{dx} + [L_p S\ (\Delta P - \sigma\ \Delta\pi)\ .\ Concentration)] \quad \textbf{(10)}$$

$$J_s = -D\ A\ \frac{dc}{dx} + [L_p S\ (\Delta P - \sigma\ \Delta\pi)\ .\ \Delta C)] \quad \textbf{(11)}$$

where σ is the Staverman's osmotic reflection coefficient describing the physical meaning of wave reflection based on the incident amplification when it is passing the barrier with no leakage of the total amplitude [47]. Its value is in the range of [0, 1], where [44] [48]:

- σ = 0 means that there is no reflection at the barrier and that the membrane is impermeable for small molecules (no osmatic pressure σ $\Delta\pi$):

$$J_v = L_p S(P_c - P_i) \quad \textbf{(12)}$$

This case explains the reflection level in organs at the end of arteries. Conductivity starts from the heart with maximum value. Then it is gradually decreasing when the plasma left the heart. So, it has a relatively inverse relationship with artery length for example liver has very low $P_c \propto \frac{1}{lenght}$.

- σ = 1 means 100% reflection at the membrane and that there is no leakage of the specified solute [47]. It is a fully osmotic pressure case where the barrier is semi-permeable, for water only, not allowing any proteins to cross the barrier [48]:

Free permeable molecules:

$$J_v = L_p S[(P_c - P_i) - (\pi_c - \pi_i)]. \quad \textbf{(13)}$$

Accordingly, this equation explains the reflection level in the organs near to the heart:

When $J_v$ is positive, the fluid flows from the capillary into the interstitial space.

In contrast, when $J_v$ is negative, the extravascular space will reabsorb the fluid coming from the intravascular space. In the special case of balance, the lymph flow is at steady state with the flux of volume rate of solute from the capillary, i.e., $J_v$ = L [43].

Macromolecular transportation (portions, antibody sand drug delivery) follows a filtration force when the conductive flux is the highest force on the wall into the interstitium, reaching the illness tissue area [45]. On the other hand, the volume of interstitium space gradually increases with this effort. Diffusion and filtration of fluid conductive pathways are basically different types of transportation when comparing the fluid size and the selectivity of the fluid via the pore sizes. For large molecules, it is going to transport through the transcellular pathway (through membrane: porters or channels) while for small size molecules, it is going to take the paracellular pathway (passive but elective variable and regulated), as in Figure 8.

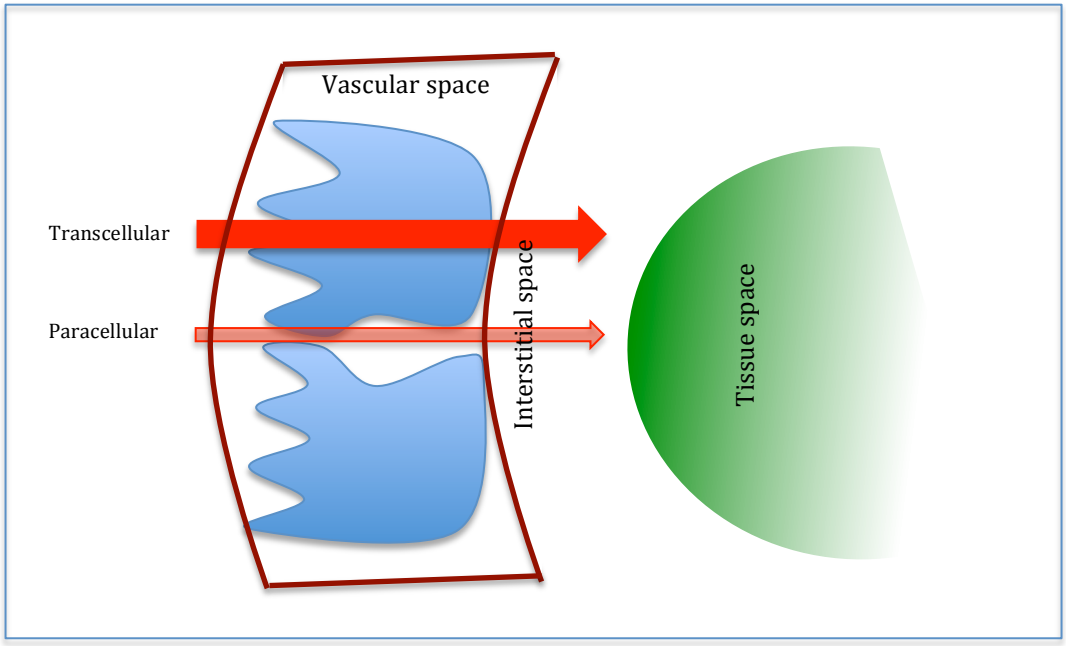


Figure 8: Fluid conductive pathways.

### 3.1.2 Two-Pore System Exchange:

In general, a two-pore system is a specific case of a volume fluid flow across a micro-wall capillarity space. In macromolecular (large-solute) transportation, it is difficult for fluid to flow easily through the endothelial layer, particularly because of molecule size and how it can move through this barrier. A physiological understanding of the vascular exchange that happens during the circulation route is essential in order to modulate it and study the transportation among different spaces. That barrier is a porous medium, which we assume to be a *heteroporous* (a mix of large and small pores) vascular system for a simple model of transportation.

The first two-pore formula was published in 1994 for solute exchanging through transcapillary, emphasizing the law of Starling [44]. It was stated that the IgG antibody uptakes into tissues through a two-pore barrier, and diffusion is negligible through “large

pores" and "small pores" within the vascular and interstitial spaces [46]. Then, systemically, B. Rippe and B. Haradsson formalized it [38]. The general equation of fluid transportation for a two-pore membrane system is given as:

$$J_v = \sum_{i=1}^{m} J_{v,i} = \sum_{i=1}^{m} \alpha_i L_p S(\Delta P - \sum_{j=1}^{n} \sigma_{i,j} \ \Delta\pi_j) \qquad \textbf{(14)}$$

where $m$ is the number of different-sized pores and $n$ is the number of solutes in the system. $\sigma_{i,j}$ is the net osmotic reflection coefficient ($\alpha_i$ is the fraction of hydraulic conductance attributed to pore type "$i$"), $L_pS$ is the capillary hydraulic conductance, $\Delta P$ is the transendothelial difference for solute "$j$" at pore type "$i$", and $\Delta\pi_j$ is the transendotheial osmotic pressure difference of solute "$j$". In a two-pore system:

$$J_{v,O} = J_{L,O} + J_{s,O} \qquad \textbf{(15)}$$

In accordance with this equation, the model can be built-up for special molecule transportation based on the concept of Sieve's molecular effect [38] [44]. In this systemic modeling, antibodies follow the transportation to each organ through the two-pore system (large and small pores).

$$J_s = J_{v,O} - DA\frac{dc}{dx} \qquad \textbf{(16)}$$

$$J_{s,O} = \left(J_{L,O} + J_{s,O}\right) - DA\frac{dc}{dx} \qquad \textbf{(17)}$$

$$\begin{aligned} J_{s,O} = &\left[J_{L,O}(1 - \sigma_L)C_{v,O} + PS_L\, Pe_{L,O}\left(C_{v,O} - \frac{C_i^F}{R_0}\right)\left(\frac{Pe_{L,O}}{e^{Pe_{L,O}} - 1}\right)\right] \\ &+ \left[J_{s,O}(1 - \sigma_s)C_{v,O} + PS_s\, Pe_{s,O}\left(C_{v,O} - \frac{C_i^F}{R_0}\right)\left(\frac{Pe_{s,O}}{e^{Pe_{s,O}} - 1}\right)\right] \end{aligned} \qquad \textbf{(18)}$$

Accordingly, the movement of molecule exchanges determines certain transportation parameters of the system. In a normal or a tumour model, there are three main parameters:

- Permeability factor P ($\frac{Cm}{S}$), constant of hydraulic conductivity$L_p$($\frac{Cm}{mm\ Hg.S}$), and osmotic coefficient reflection σ.
- Surface area S ($cm^2$) of transport exchanging.
- Transported concentration and pressure gradients P and $\pi$ (mm Hg) [42].

## 3.2 Compartment Modeling

The modeling of biological systems relies on the integration and the understanding of physiological and mathematical aspects. It has been developed for theoretical purposes and numerical simulations can investigate and predict the correlation between physiological processes and a mAb disposition. In different species, the pathway of non-linear disposition varies greatly.

There are many challenges to face when developing a model from simple to professional and more complicated; especially a model that also has to respect the physiological side of the biological processes within the body. These studies considered factors that could manipulate the roles of the administration route, molecular size and weight, pH level, and toxicity level.

There are two types of studies that can describe the biological interactions of any drug, Figure 9. First, a pharmacokinetics (PK) study, which aims to understand how concentration changes as it moves through the body in different compartments, tissues, or organs, and to describe what the body does with the drug from its point of entrance

(through intravenous, subcutaneous, inhalation or oral administration) until its exit. Second, a pharmacodynamics (PD) study, on the other hand, investigates how the drug affects the body and gives the drug-receptor interaction. So inversely, this can give the drug-receptor interaction to explain, "what does the drug do to the body?", i.e., the level of efficacy. The PK/PD process clarifies the mechanisms of antibody development and the identification of appropriate dose regimens [49].

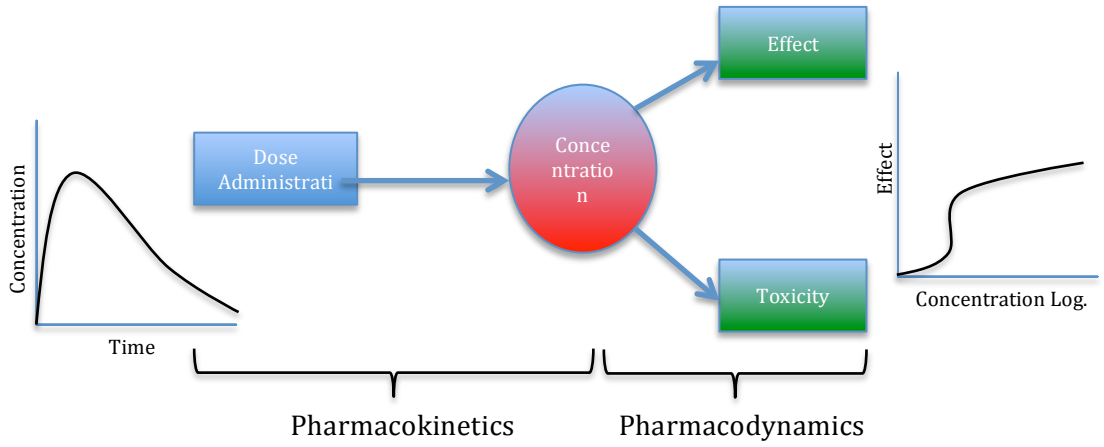


Figure 9: PK/PD general process flow.

**P**hysiology-**B**ased **P**harmaco**k**inetics (PBPK) is one of the mathematical models that describe the hybridoma technique and the engineering design of macromolecules (proteins, dextrans, polymer beads, and DNA) and small molecules used as diagnostic and therapeutic particles [50][51]. It can describe the bio-distribution of macromolecule drugs in terms of the time course of the drug ADME (**A**dministration, **D**istribution, **M**etabolism and **E**limination "Excretion") [50]. The drug's actions are studied during its administration, in order to monitor the distribution and the concentration. This study cannot be achieved directly from a data collection; the information has to be taken from samples of blood, plasma, urine, saliva, and/or other corporal fluids. The first

Physiologically-Based Pharmacokinetic PBPK model was proposed by Covell *et al*. in 1986. It was developed for six organs – lung, heart, liver, spleen, kidney and carcass- and three parameters per organ, i.e., permeability, volume concentration, and constant of elimination.

The best way to study this model is to follow the developmental steps, which can be defined sequentially as:

- Model the structure,
- Select the tissues and organs to model,
- Set-up the model equations depending on the tissue/organ specific parameters, and
- Solve the system and determine the output model parameters [52].

## 3.3 Model Development

A wide variety of mathematical models have been developed to evaluate different approaches to radioimmunotherapy. Such modeling has been used to evaluate the use of unlabeled (cold) antibodies to (i) saturate antigen sites in the liver or spleen and thereby improve the radioimmunodiagnosis or the radioimmunotherapy, (ii) examine the differences between intact antibodies and antibody fragments with regard to distribution, catabolism, and excretion, (iii) understand the effects of circulating antigen on the antibody model design distribution, (iv) optimize two-step approaches, (v) optimize administered amounts, and (vi) simulate plasmapheresis or extracorporeal immunoadsorption to improve therapy or diagnosis by clearing the plasma of excess unbound antibodies.

## 3.4 Conclusion

In this work, we focused on two kinds of models to perform a comparative study and determine the improvement in a body when we conjugated the IgG with Amifostine. The first model, taken as reference model, is a two-compartment model for the two-pore concept of molecular exchange. This model was published in 2001 [4] to study the effective parameters for IgG antibodies and its fragments. The second model is a model we developed to investigate the *immuno-radioprotector* molecule behavior and study the pharmacokinetics profile of a toxic drug (Amifostine) in terms of a three-compartment model. It represents the function of a compartment physiology model that consists of a peripheral compartment (normal tissue) and a central compartment (targeted tumour interstitial; free and bound Ab). Each compartment has a specific dependent parameter equation describing the bio-distribution. In some systems, we could have more than one equation per compartment because of the physiological delivery of the drug (free Ab and bound Ab). Thus, equations have to be mathematically balanced by mass-balance [53]. Essentially, we extracted the equations describing the proposed releasing third compartment based on the mass-balance principle using the reference model's equations. The equations describe the change of concentration of a drug, receptor, and drug receptor complex in the central and peripheral compartments. There are also specific quantities called "error parameters" whose role is to determine the frames of mass equilibrium ($K^f$, $K^r$and$K_e$), thus be either positive or negative. Chapter 4 will provide more details concerning the whole framework of these models.

# Chapter 4. Mathematical Modelling, Simulation Procedure and Data Acquisition

The developed models are based on specific parameters that can affect the time-dependant concentration profile C(t). In fact, the mass transfer and reaction phenomena describe the ADME of each molecule when it is infused in the body while each organ is described as a compartment model that can be systemically formulated as an **O**rdinary **D**ifferential **E**quation (ODE). Therefore we solved numerically this ODE to get the concentration profile C(t) for each compartment in the system, using the MATLAB 2014b simulation tool [50].

Then, we studied the unsteady-state of transportation and the effect of the drug in the body as pharmacokinetic. The parameters of the system were classified into physiological parameters and compound-specific (kinetic) parameters. In this case of dynamic mass model, we represented the targeted (tumour) and eliminated (liver) organs. At the end of this exchange, the system should return to its steady state equilibrium, which can take a couple of days with little change in the bio-distribution [54]

## 4.1 Physiological Parameters

The physiological parameters are the volumes of each tissue/organ as spaces or sub-compartments. Modeling, which implies both biological and physiological sides, involves mathematical equations that describe physiology processes related to bio-distribution of molecule. Physiological parameters include volumes of compartment after weighted [54], flow rates into/out the compartment, and lymph flow rate [45].

### 4.1.1 Compartment volumes of the system

The antibody concentration from vascular space to target tissue must be under order of transportation. To evaluate it, we have to know how the rate will be through different spaces of compartments such as the total tissue volume ($V_{tot}$), the vascular volume ($V_{v,\,o}$), and the interstitial volume ($V_{i,\,o}$). Note that $\boldsymbol{V_{tot,O} = V_{V,O} + V_{i,O} + V_{N,O}}$ (table 4-1).

Table 4-1: Physiological parameters for tumour and liver.

| | **Tumour** | **Liver** |
|---|---|---|
| **Total tissue volume $\boldsymbol{V_{tot,O}}$ (ml)** [4] | 20 | 1809 |
| **Vascular volume $\boldsymbol{V_{V,O}}$ (ml)** [4] | 1.4 | 181 |
| **Interstitial volume $\boldsymbol{V_{i,O}}$ (ml)** [4] | 10.9 | 362 |
| **Normal volume $\boldsymbol{V_{N,O}}$ (ml)** | 20 - (1.4 + 10.9) = 7.7 | 1809 - (181 + 362) = 1266 |
| **Plasma flow $\boldsymbol{Q_O}$ (ml $\boldsymbol{g^{-1}S^{-1}}$)** [4] | 0.1 | $7.4 \times 10^{-3}$ |
| **Lymphatic flow $\boldsymbol{L_O}$ (ml $\boldsymbol{g^{-1}S^{-1}}$)** [4] | 0 | $7.7 \times 10^{-6}$ |
| **Fluid Recirculation flow rate $\boldsymbol{J_{iso,o}}$ (ml $\boldsymbol{g^{-1}S^{-1}}$ )** [4] | $10.8 \times \mathbf{10^{-5}}$ | $43 \times \mathbf{10^{-5}}$ |

### 4.1.2 Transporting parameters

Some of the other parameters can be classified depending on the route transportation through the pores and in different organs (table 4-1). These parameters affect the isogravimetic flow rate $\boldsymbol{J_{iso,o}}$ that is related to the net flux of volumetric flux rate and starling forces (P and $\pi$) [50].

1- Organ physiological parameters:

Fluid recirculation flow rate $J_{iso,O}$ (i.e.,$J_{iso,Tumor}$, $J_{iso,Liver}$), figure 10, plasma (blood) flow rate ($Q_O$; $Q_{Tumor}$, $Q_{Liver}$) and lymphatic flow rate ($L_O$; $L_{Tumor}$, $L_{Liver}$) are flow rate quantities that explain the hypothesis of blood in extravasation. $J_O$ is the input rate specified for the exchange point of the molecule via two-pore system from the vascular space to interstitial space [50].

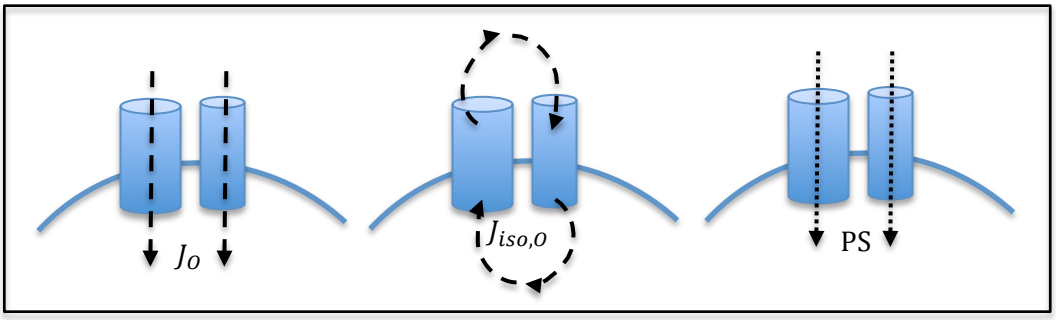


Figure 10 Parameter behaviors showing the exchange of molecule through heteropore system. [50]

They indeed give information about the route of antibody molecule while considering the flow rate of the molecule arriving to tissue and lymph vessel (and also leaving the tissue). In tumour, there is no value for lymphatic system because fluid oozes the tumour by elimination in periphery [56].

2- Amifostine and antibody physiological parameters

Macromolecule (Amifostine and Ab) has specific physiological parameters which can address the molecule as a well-known particle. For Amifostine, the recommended clinical dose in radiotherapy starts by considering the Body Surface Area (BSA, $mg/m^2$). According to Dr. Steven Halls' BSA calculator [57], we can extract the dose in (mg) for reference body [58]. The calculation of the Amifostine dose 15-min i.v. infused was obtained from (table 4-2) and the tolerance dose in (table 4-3):

$$Medication\ Dose\ (mg) = BSA\ (m^2) \times Administration\ Dose\ (\frac{dose}{m^2}) = 1.97\ m^2 \times 910\ \frac{mg}{m^2}$$

$$= 1792.7\ mg\ for\ reference\ man\ 80kg$$

For the antibody, the parameters were based on clinical data collected to study the bio-distribution of carcinoembryonic antigen (CEA) (table 4-4) [4]. Note that these parameters are for the IgG-antibody when it was conjugated with radiolabelled with $^{131}I$ to follow it and detect it (by imaging the molecule in the biological media).

Table 4-2: Amifostine physiological parameters.

| **Body Weight Reference BW (kg)** | **60 Kg** | **80 Kg** |
|---|---|---|
| **Body Surface Area BSA (m2) [58]** | 162 $m^2$ | 1.97 $m^2$ |
| **Administration dose (mg/kg) [58]** | 24.3 mg/kg | - |
| **Administration Dose (mg/m2) [58]** | 500-910 $mg/m^2$ | 910 $mg/m^2$ |
| **General Dose (mg) (calculated)** | 1456 mg | 1792.7 mg |
| **Plasma ($\alpha$) (min) [58]** | ~10 min | - |
| **Peak plasma level of WR-1065 (µM) [58]** | 100 µM | - |
| **T1/2$\beta$ (hr) [58]** | >2 hr | - |

Table 4-3: Specific pharmacokinetics based on the dose tolerance [17].

| **Maximum tolerated dose (MTD)** | 740 mg/m2 (i.v) | 910 mg/m2 (i.v.) |
|---|---|---|
| **Area Under Curve AUC (mmol/L.h)** | 90.36 | 231.12 |
| **Distribution volume $V_d$ (L)** | 8.7 L | 7.4 L |
| **Maximum plasma concentration $C_{max}$(mmol/L)** | 0.100 | 0.235 |
| **Plasma clearance C (L/h)** | 258 L/h | 126 L/h |
| **Plasma half-life $\alpha$ (min)** | 1.5 min | 2.7 min |

Table 4-4: Antibody physiological parameters [4].

| Physiology parameter for CEA-IgG | IgG Data |
|---|---|
| **Effective radius r ($A^0$)** | 540 nm = $54A^0$ |
| **Reflection coefficient $\sigma_S, \sigma_L$** | $\sigma$S= 0.944 $\sigma$L= 0.056 |
| **Concentration of antigen in the tumour a (M)** | 10-8 M |
| **Permeability $PS_L, PS_S$** | $PS_S$=10-6 $PS_l$=10-6 |
| **Molecular Weight MW (KDa)** | 150 KDa |
| **Alpha half-life for plasma (hr)** | 2.3 hr |
| **Beta half-life for elimination (hr)** | 26.0 hr |

## 4.2 Kinetic Parameters and other mixed parameters

Kinetic parameters include the equilibrium constants for antibody attaching the receptor and detachment for non-specific (i.e. liver) and specific (i.e. tumour) organs. Those parameters in tumour are the association rate constant for antibody per unit time $K_t^f$ ($M^{-1}min^{-1}$), the Dissociation rate for antibody $K_t^r$ ($min^{-1}$), and the Catabolic elimination rate - for each organ - $K_{e,t}$(ml $min^{-1}$) from interstitium space [4] (table 4-5). In antibody molecule, the dissociation rate constant is the inverse of the affinity ($K_a = 1/K_t^r = 0.196 \times 10^5$), a very distinguish parameter to test and know how strong is the given bound between an antibody Ab and its antigen Ag [50]. In contrast, these

parameters are not applicable to liver because liver is an elimination organ based on the physiology of protein clearance from the body. The determined parameters are summarized in table 4-1.

Table 4-5: Kinetic parameters.

| | **Tumour** | **Liver** |
|---|---|---|
| **Affinity constant = 1/$K_t^r$ ($M^{-1}$)** | $0.196 \times 10^5$ | 0 |
| **Association $K_t^f$ ($M^{-1}min^{-1}$) [4]** | $3.6 \times 10^5$ | 0 |
| **Dissociation $K_t^r$ ($min^{-1}$) [4]** | $5.1 \times 10^{-5}$ | 0 |
| **$K_{e,t}$ ($S^{-1}$ $10^{-6}$) [4]** | 53 | 0 |

## 4.3 Developed mathematical model:

The system has to take into account the mass balance in pharmacokinetic model with high faithful of compartments interconnected anatomically [55]. As mentioned, the first developed model is basically a two-compartment model, which can be used to determine a given design for antibody-based target therapy [4]. The aim was to use it to perform a comparative study with the main model we developed for this work. Because the system is physically transportation of particle in the pipe, we were concerned about the molecular volume of this particle after conjugation (Amifostine-antibody = *immuno-radioprotector* molecule). Hence, we carefully investigated all parameters to know how they vary when the molecule becomes larger. The particle size of macromolecule is

physically represented as a spherical volume shape. IgG radius in the model assumed that MW $\propto r^3$[4].

4.3.1 Flux of fluid flow through heteropore microvascular walls:

The next step was to setup an equation for each compartment of the model to describe the full frame of molecule's transport. The equations should be inter-dependent by sharing common parameters. Assuming this, each compartment of the system will be well mixed and with uniform distribution. That will lead to a full system of equations with the concentration as function of time. The initial condition of the system is zero for the model. As previously mentioned, the mathematical concepts behind the model are:

the Starling's Law of Capillaries from (15):

$$J_{L,O} = J_{iso,O} + \alpha_L L_O$$
$$J_{S,O} = -J_{iso,O} + \alpha_S L_O \quad \textbf{(19)}$$

with, $J_{L,O}$+$J_{S,O}$= Net flow ($J_O$), and $\alpha_L + \alpha_S$=1

$$J_{iso,O} = \alpha_L \alpha_S L_p S\,(\sigma_S - \sigma_L)(\pi_V - \pi_i) \quad \textbf{(20)}$$

For our model, let m = 2 (two pore quantities in the system: small and large) and n = 1 (only one infused molecule). Then (18) can be reformulated as:

$$J_{solute,L,O} = \left[ J_{L,O}(1 - \sigma_L) C_{v,O} + PS_L\, Pe_{L,O} \left( C_{v,O} - \frac{C_i^F}{R_0} \right) \left( \frac{Pe_{L,O}}{e^{Pe_{L,O}} - 1} \right) \right]$$
$$J_{solute,s,O} = -\left[ J_{s,O}(1 - \sigma_s) C_{v,O} + PS_s\, Pe_{s,O} \left( C_{v,O} - \frac{C_i^F}{R_0} \right) \left( \frac{Pe_{s,O}}{e^{Pe_{s,O}} - 1} \right) \right] \quad \textbf{(21)}$$

4.3.2 Mass balance and rate exchange equations for IgG:

From the pharmacokinetics model, the molecule circulation throughout the system is described by the mass balance equation. Each organ (tumour and liver) in this model

can be classified into two compartments. The vascular space is for the free Ab-molecule while the extravascular space is for both binding: Ab-molecule and free Ab-molecule. On the other side, equilibrium across the capillary between the plasma fluid and the interstitial fluid is under the rule of the two-pore theory [55]. Then we have two main systems for i.v. administration, IgG system and *immuno-radioprotector* system, are Pk model. Both models of each organ set as one system: targeted model (tumour) and elimination model (liver), see figure 11. In the PK model, we need to define the initial concentration in the plasma of the administrated drug. The molecular concentration in the plasma (Cpl) is indeed one of the key parameters in the system. It is given as:

$$C_{pl} = C_0 \left(e^{-\lambda_1 t} + e^{-\lambda_2 t}\right)$$

where $C_0$ is the initial concentration of administrated molecule i.v. with $C_0 = \frac{Dose}{Volume}$. It was set as 1792.7 mg (tables 4-1 and 4-2). The half-lives for this molecule are given by (Table 4-6):

$$T_\alpha = \frac{\ln(2)}{2}$$

$$T_\beta = \frac{\ln(2)}{2}$$

Table 4-6: Ab half-lives [4].

| | **IgG-Ab** |
|---|---|
| **Beta half-life $T_\beta$** | 120 min |
| **Alpha half-life $T_\alpha$** | 1560 min |
| **$C_0$** | $C_0 = \frac{1792.7\ mg}{20\ ml}$= 89.635mg/ml |

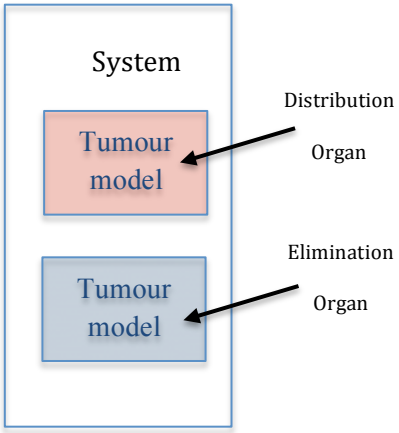


Figure 11: Pharmacokinetics system for two organs (tumour and liver).

- Tumour model (Targeted tissues):

The tumour model is the targeted area in this work. The tumour vascular has unique bio-physiological structure that can be classified into two main parts: peripheral and central. The first is the vascularization region while the central part has a very poor distribution of vascular, figure 12 [42]. The slandered vascular distribution in normal tissues (artery to capillaries to vein) is not normally uniform but stochastic.

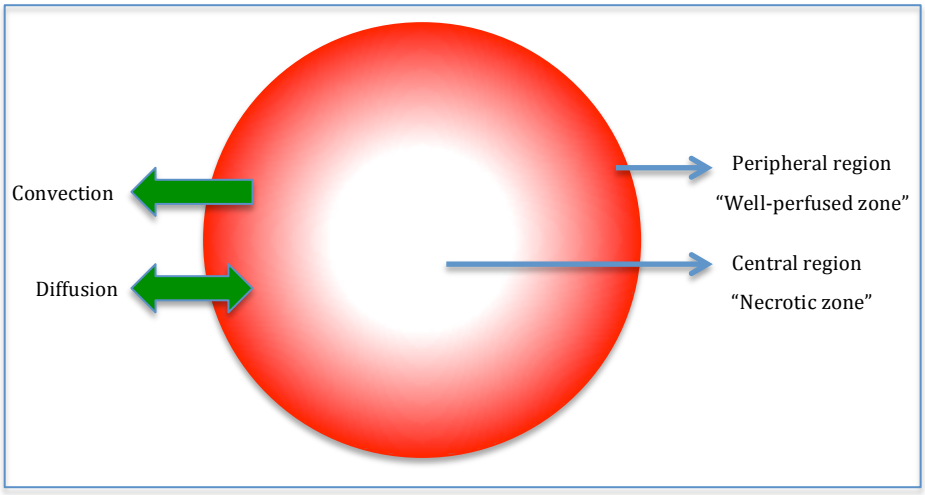


Figure 12: The distribution of vascularization zones in tumour.

The transportation of IgG-antibody and the concentration in the system were considered for each compartment. In this model of two-compartments, there are two main rates to consider: one for the first compartment of normal tissue in vascular space and the second for the interstitial space, which requires two formulations for free antibody and for bound antibody, respectively.

Therefore, this latter compartment was divided into these two parts to meet the physiological paths of antibody. Such formulas are first-order differential equations based on figure 12.

Normal tissue equation for antibody concentration in vascular space:

$$V_{v,t}\left(\frac{dC_{v,t}}{dt}\right) = Q_t C_{pl} - (Q_t - L_t)C_{v,t} - J_o \qquad \textbf{(22)}$$

Tumour Tissue equations for free antibody and bound antibody concentration in interstitial space:

$$V_{i,t}\left(\frac{dC_{i,t}^{f}}{dt}\right) = J_o - K_t^f C_{i,t}^f V_{i,t} + K_t^r C_{i,t}^B V_{i,t} - L_t C_{i,t}^f$$

$$V_{i,t}\left(\frac{dC_{i,t}^{B}}{dt}\right) = K_t^f C_{i,t}^f V_{i,t} - K_t^r C_{i,t}^B V_{i,t} - K_{e,t} C_{i,t}^f V_{i,t} \qquad \textbf{(23)}$$

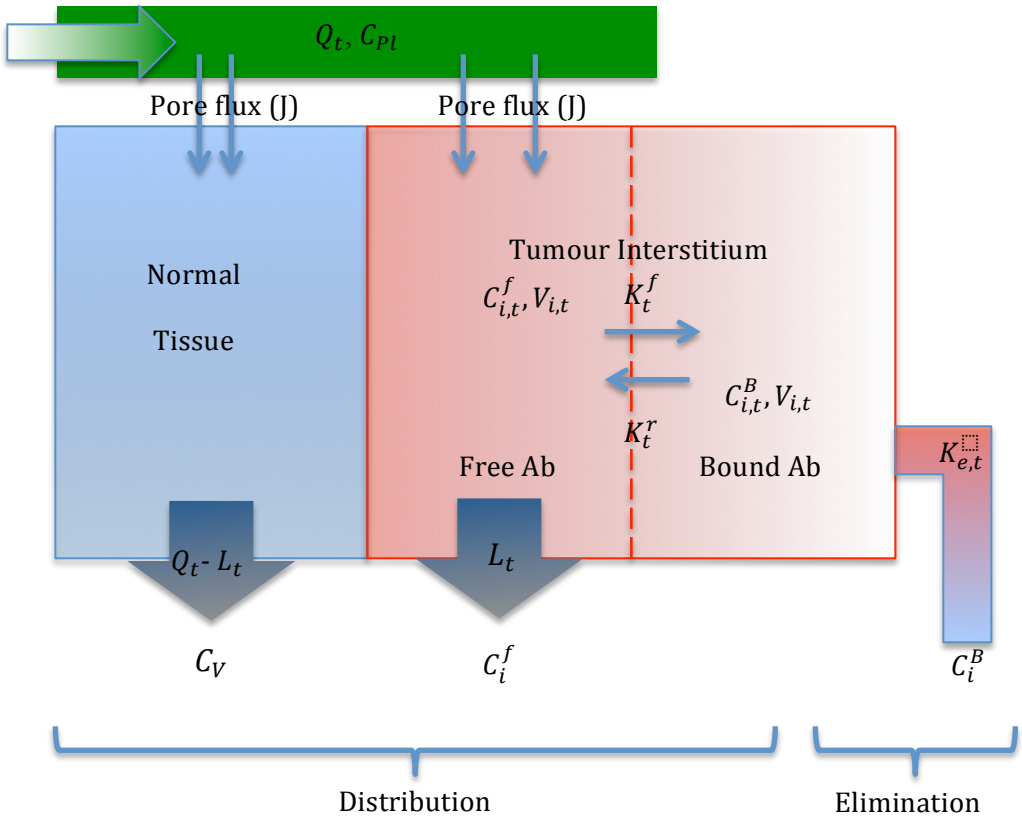


Figure 13. Antibody transportation in a two-compartment model in tumour [4].

- Liver model:

The liver model follows the same classification of compartment and parameters as an organ of the system of biological body, figures 13 and 14.

First compartment for normal tissue:

$$V_{v,l}\left(\frac{dC_{v,l}}{dt}\right) = Q_l C_{pl} - (Q_l - L_l)C_{v,l} - J_o \qquad \textbf{(24)}$$

Second compartment for interstitial tissue:

For free Ab

$$V_{i,l}\left(d\frac{C_{i,l}^{f}}{dt}\right) = J_o - K_l^f C_{i,l}^f V_{i,l} + K_l^r C_{i,l}^B V_{i,l} - L_l C_{i,l}^f \quad \textbf{(25)}$$

For bound Ab

$$V_{i,l}\left(\frac{dC_{i,l}^{B}}{dt}\right) = K_l^f C_{i,l}^f V_{i,l} - K_l^r C_{i,l}^B V_{i,l} - K_{e,l} C_{i,l}^B V_{i,l} \quad \textbf{(26)}$$

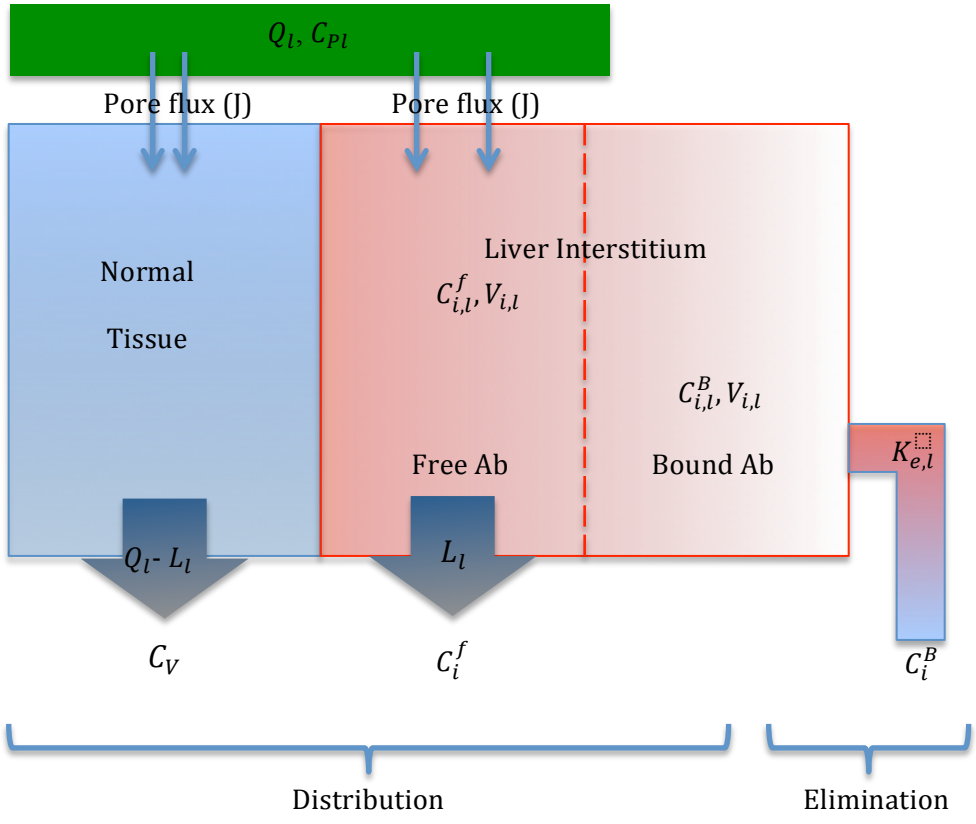


Figure 14: Liver model for IgG antibody molecule.

### 4.4 *Immuno-radioprotector* model

As previously detailed, the *immuno-radioprotector* model has basically the same physiological parameters. The tumour model is the main model of the system because from here we can observe the bio-distribution of *immuno-radioprotector* molecule from the targeted area of radiotherapy (tumour) beside the protection area (the one we

introduced). From here, a more precise designed model was needed for the protection compartment. Therefore, we introduced a three-compartment system was a better approach to explain the operation of this molecule according to the physiology and the mass balance (as compared to the original model with two-compartments).

- Tumour model:

Vascular space equation in tumour:

$$V_{v,t}\left(\frac{dC_{v,t}}{dt}\right) = Q_t C_{pl} - (Q_t - L_t)C_{v,t} - J_o \qquad \textbf{(27)}$$

Interstitial space in tumour, *immuno-radioprotector* compartment:

$$V_{i,t}\left(\frac{dC_{i,t}^{f}}{dt}\right) = J_o - K_t^f\, C_{i,t}^f(\frac{V_{i,t}}{2}) + K_t^r\; C_{i,t}^B\,(\frac{V_{i,t}}{2}) - L_t\; C_{i,t}^f \qquad \textbf{(28)}$$

Assuming that $V_{i,t}$will be half volume of interstitium space $\frac{V_{i,t}}{2}$ of tumour volume.

Bound *immuno-radioprotector* compartment:

$$V_{i,t}\left(\frac{C_{i,t}^B}{dt}\right) = K_t^f\, C_{i,t}^f\, V_{i,t} - K_t^r\; C_{i,t}^B\, V_{i,t} - K_{e,t}\; C_{i,t}^B\, V_{i,t} \qquad \textbf{(29)}$$

The new compartment (working as a normal tissue around the treatment area) is the compartment where the incident antibody from tumour tissues will be either bounded or free in the interstitium compartment (free antibody interstitial compartment$C_{i,t}^f$), as shown in figure 15.

Protection area of *immuno-radioprotector* molecule in normal tissue:

$$V_{N,t}\left(\frac{d\; C_{N,t}^f}{dt}\right) = \; K_t^{f'}\, C_{i,t}^f\, V_{N,t} - \; K_{e,t}'\; C_{N,t}^f\, V_{N,t} \qquad \textbf{(30)}$$

assuming that: $K'_{e,t}$ =$K_{e,t}$ and $K_t^{f\prime}$ = $K_t^f$ (table 4-6).

Table 4-7: Values for the new compartment.

| **Fixed parameter project** | |
|---|---|
| $\boldsymbol{K'_{e,t}}$ $(\boldsymbol{S^{-1}})$ | 53 |
| $\boldsymbol{V_{N,t}}$ $(\boldsymbol{ml})$ | $V_{N,t}$ =$V_{tot,t}$-($V_{i,t}$+$V_{v,t}$) = 20 – (10.9 + 1.4)= 7.7 |
| $\boldsymbol{K_t^{f\prime}}$ $(\boldsymbol{M^{-1}S^{-1}})$ | 3.6 × $10^5$ |

- Liver model:

Vascular space in liver:

$$V_{v,l}\left(\frac{C_{v,l}}{dt}\right) = Q_l C_{pl} - (Q_l - L_l)C_{v,l} - J_o \qquad \textbf{(31)}$$

Interstitial space in liver (free and bound molecule):

$$V_{i,l}\left(\frac{C_{i,l}^f}{dt}\right) = J_o - K_l^f C_{i,l}^f(\frac{V_{i,t}}{2}) + K_l^r C_{i,l}^B(\frac{V_{i,l}}{2}) - L_l C_{i,l}^f \qquad \textbf{(32)}$$

$$V_{i,l}\left(\frac{C_{i,l}^B}{dt}\right) = K_l^f C_{i,l}^f V_{i,t} - K_l^r C_{i,l}^B V_{i,l} - K_{e,l} C_{i,l}^B V_{i,l} \qquad \textbf{(33)}$$

New compartment's equation where the protection equation of normal tissue:

$$V_{N,l}\left(\frac{d\, C_{N,l}^f}{dt}\right) = K_l^{f\prime} C_{i,l}^f V_{N,l} - K'_{e,l} C_{N,l}^f V_{N,l} \qquad \textbf{(34)}$$

All above equations consist of two main terms that describe the full clearance into bio-distribution (rapid clearance) and elimination (slow clearance) for each compartment. These are the two-step equations that have the bi-exponential decays ($\alpha$ and $\beta$). For

example, equation (34) has two terms of clearance: one for bio-distribution ($K_l^{f'} C_{i,l}^f V_{N,l}$) and one for elimination ($K'_{e,l} C_{N,l}^f V_{N,l}$).

### 4.5 Drug-dependent parameters:

Starting from the logic of adding a drug to an antibody, we had to calculate the total mass while combining both of them; this is the molecular weight MW. In our case, the total molecular weight of *immuno-radioprotector* molecule can be obtained as:

$$MW_{tot} = MW_{Ab} + MW_{amifostine}$$

$$= 150 \text{ kDa} + 0.215 \text{ kDa}$$

$$MW_{tot} = 150.215 \text{ kDa}$$

Form the result we can observe that the total molecular weight of *immuno-radioprotector* is almost nothing comparing with the antibody weight. Therefore, we neglected the effect of MW increasing (less than 0.15% change in the total mass of the molecule). So, the effective radius of the molecule will remain approximately the same.

In this work, several key drug-dependent parameters could be considered: (i) the reflection coefficient of the molecule transportation for small and large pores $\sigma_S$,$\sigma_L$ respectively, (ii) the permeability of cell surface to leave the molecule and pass the barrier for each pore$PS_L$,$PS_s$ ($min^{-1}$), (iii) the association rate constant for binding Ab ($M^{-1}S^{-1}$), and (iv) the total dose of drug (mol) [59].

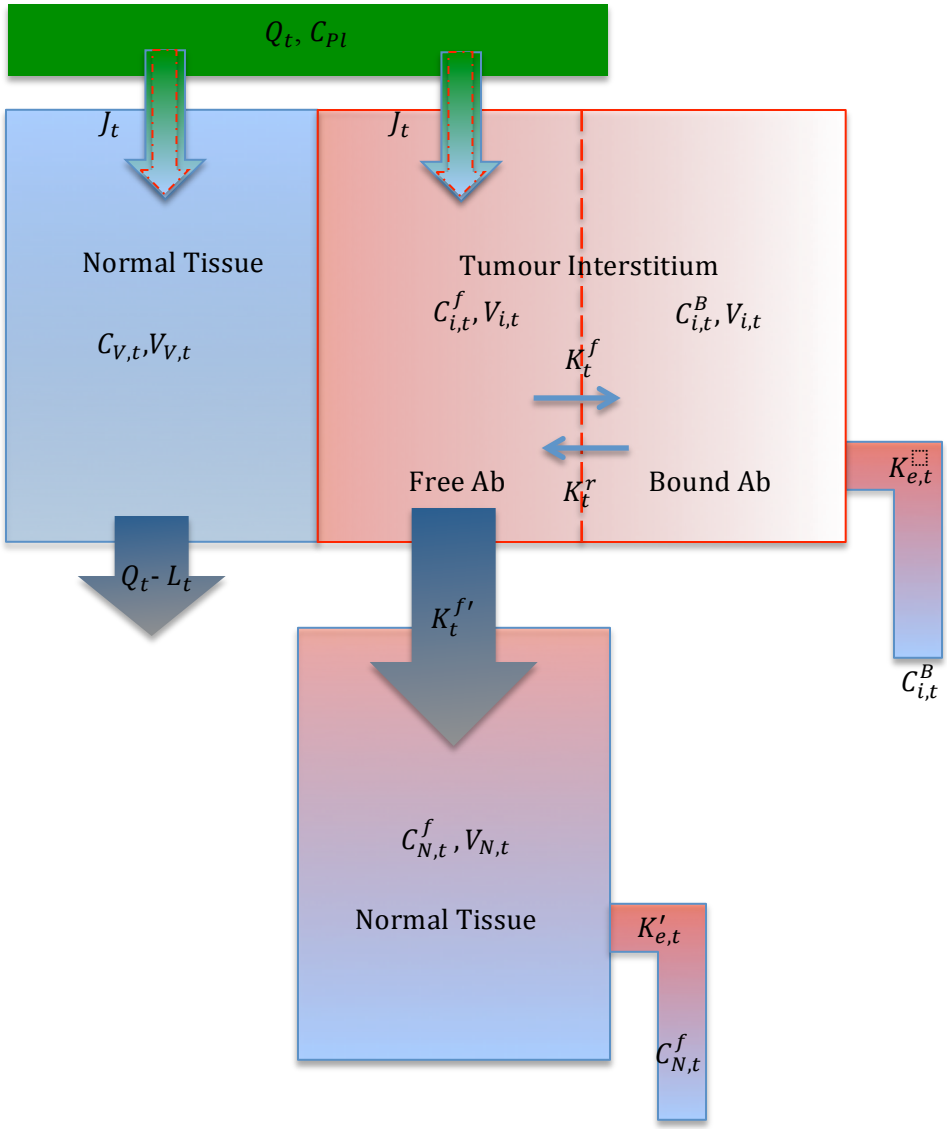


Figure 15: Hypothesis model for *immuno-radioprotector* transportation through two-pour system in three-compartment model.

We, therefore, investigated the influence of these parameters on the system. We varied them one by one, keeping in mind that the molecule should not significantly change. Indeed, it still has all the features of antibody with no significant change in the molecular mass.

Let us consider first the reflection coefficient in two-pore system. It is in the range of [0, 1] with $\sigma_S+\sigma_L = 1$. However, since the reflection is mainly related to the volume of the molecule, it will not vary in our case (the protein transportation doesn't affect the molecule mass and volume).

Permeability of each pore ($PS_L$ , $PS_s$) is the second parameter that has a relationship between the surface area of transportation and the ability of passing this area. Since permeability is the same in proteins, it will not change because both molecules are proteins.

The next parameter is related to the antibody association rate. It is a constant for the antibody protein particle. Accordingly, it will remain the same as in the original model unless we will use different kinds of antibody.

The last parameter that we may have to consider here is the total dose administration, which is an input variable in this model. However, without practical data from hospitals, we took normalized values for your inputs.

## 4.6 conclusions

In this chapter, we presented a set of pharmacokinetics parameters (physiological and kinetic) needed to evaluate the models. The integrated method combines the drug (Amifostine) and antibody (IgG) as one protection agent. This *immuno-radioprotector*, or agent of protection, is designed to overcome the problems of use limitation of Amifostine in radiotherapy as we mentioned earlier.

Physiological data of the model, collected from different sources, were used the data of the original two-compartment model. Based on this set of physiological data, we built our new three-compartment model based on the physiological distribution mechanism of the molecule behavior. So, the physiological parameters will still the same because both systems have the same environment of studying. So kinetics parameters will remain the same as constants valid for both systems.

The next chapter will show our results in terms of concentration profiles for each organ (tumour and liver) in two systems of pharmacokinetics (reference model and proposed model).

# Chapter 5. Results

Based on the previous chapter, we developed two pharmacokinetic models. Both models have the same concept of behaviour and biological mechanism except into the metabolism stage because of the conjugated drug (Amifostine). Also, we formulated the mathematical description of each model to determine the time-varying concentration in each compartment.

## 5.1 Results

The molecule should be administrated into the system at specific dose and initial concentration. This is basically related to plasma concentration profiles that have been generated from a physiologically-based pharmacokinetic model of monoclonal antibody. It is the initial input for the system and one of the parameters in the differential equations. We can then extract the behaviour of the molecule in the plasma space (before and after the compartmental transportation part). The value of this initial concentration was set to 89.64 nM as shown in figure 16.

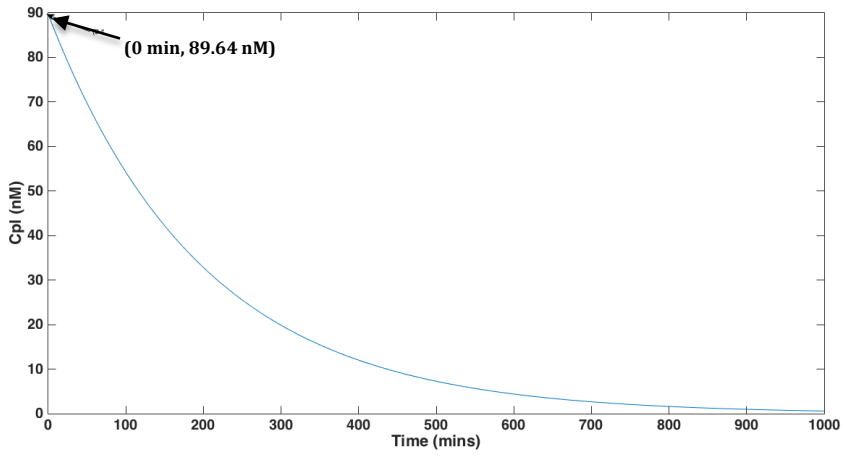


Figure 16: plasma concentration.

5.1.1 IgG model

- Tumour model:

It is a pharmacokinetic model and the reference model of this project. This two-compartment model is described with first order differential equations (Eqs. (22) and (23), chapter 4) and (i.v.) input parameters as in [4]. Parameters of these equations were determined as a relationship between volumetric distribution (V) and clearance. Ab was equilibrated during the Ab clearance from the blood (figures 16 and 17). The model was identified to determine antibody localisation by Ab affinity, flow rate of Ab clearance and elimination rate for tumour as Ab-targeted cancer therapy. The dot red curves in figures 16 and 17 are the concentration of *immuno-radioprotector* in vascular space for reference model. These results of concentration in vascular space achieved excellent agreement with observed data after simulation for the reference model.

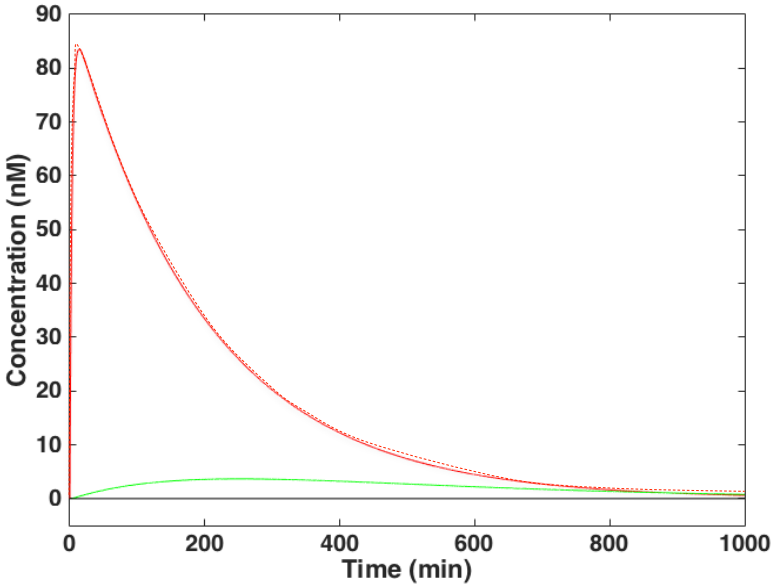


Figure 17: Concentration of Ab in vascular space (red) and the interstitium space for free antibody (black) and bound antibody (green). The dot-red curve represents the data from [4]

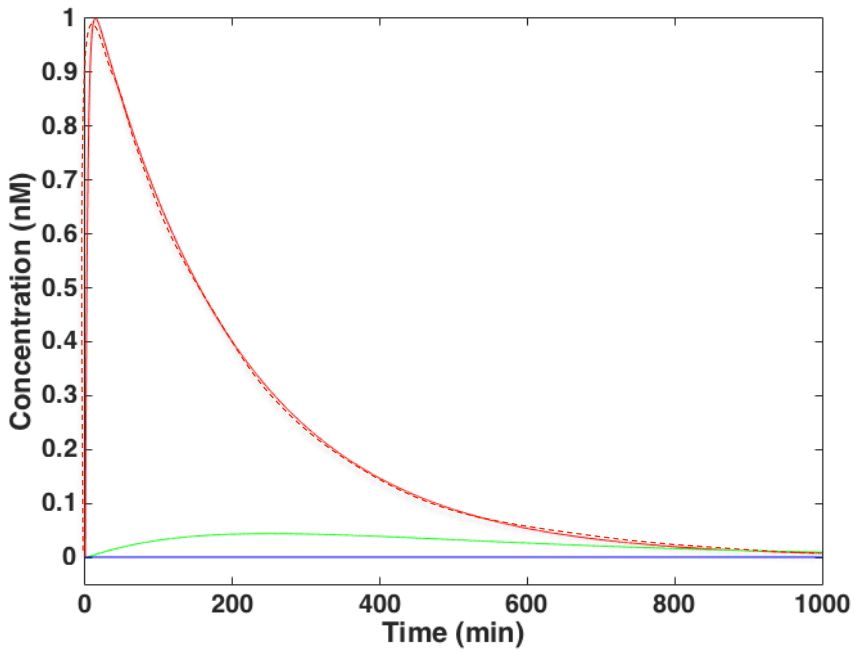


Figure 18: Full system after normalizing the concentration axis.

From figures 16 and 17, we can observe the changes of concentration per time. The red curve is overlapping with the dot red curve that was published in [4] (thus validating our model), while the two other curves (black for the free IgG and green for the bound antibody) are derived for this study using the equations in the reference. Vascular concentration shows a very sharp elimination comparing with the two other curves. That means when IgG is administrated in the system intravenously i.v. , IgG is reaching the maximum value of concentration at 13.85 min with 83.54 nM concentration. Then, the next compartment of IgG concentration was concentrated into the tumour compartment. The tumour compartment has two sub-compartments: one for free antibody $\boldsymbol{C_{i,l}^{f}}$ which is reaching its maximum concentration $1.812 \times 10^{-9}$ at 16.8 min. The other sub-compartment is for bound antibody $\boldsymbol{C_{i,l}^{B}}$that internalized to the central of tumour and increased to the maximum value concentration 3.66 nM at 251.45 min. This sub-

compartment is took the much longer time [246, 256.9] min because of the internalization and the force of association rate needed to bound the antibody.

- Liver model:

The plasma concentration-time curve of IgG has the same model structure. According to equations (24), (25), and (26), this model elimination gave values only for concentration of IgG in the vascular space and the interstitial space as one compartment because the constants of association and dissociation ($K_l^f, K_l^B$), as well as the elimination constant ($K_{e,l}$) are zero. Liver is the elimination organ of the system that eliminates the concentration of the interstitial tissue via the lymphatic flow rate ($L_l\ C_{v,l}$).

Elimination according to the half-life ($\beta$) of both molecules amifostine and IgG are 8.8 min and 1560.0 min, respectively. In the liver model, concentration in vascular space is the input volume in the first compartment then the concentration will move and be accumulated in the next compartment "interstitial space". Then the curve of second compartment in figure 18 is decreasing with time very slightly after reaching the maximum concentration at (3274 min, 0.9235 nM). This curve is almost constant with time because of the slow process of elimination where the peak is taking [3042, 3506] min. The molecular concentration in vascular compartment in figure 18 shows the excellent agreement of the data with the reference model and has the same peak maximally at (1530.55 min, 21.73 nM). Both compartments have an equilibrium point of (1792 min, 0.9066 nM) figure 18.

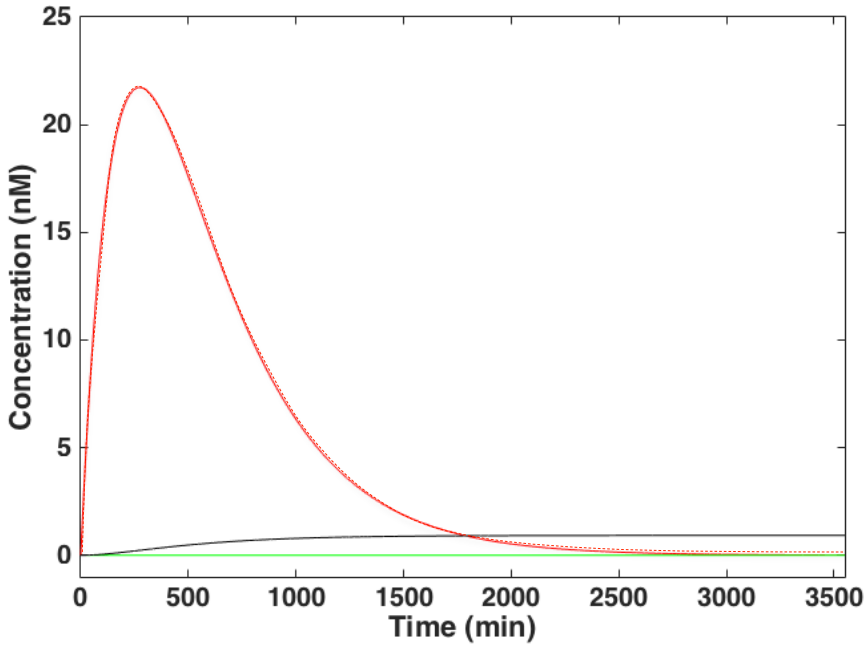


Figure 19: Concentration of liver model in IgG system. (red$\boldsymbol{C_{v,t}}$, black $\boldsymbol{C_{i,l}^{f}}$). The dot-red curve represents the data from [4]

5.1.2 *Immuno-radioprotector* model

The main proposed target of the project work is to investigate the drug behavior in the body based on the prior results of two-compartment model [4]. Physiologically, *immuno-radioprotector* molecule distributes differently in the target treatment comparing with distribution in the reference model. In fact, the third compartment was the compartment of absorption for the drug after targeting the whole molecule to the tumour and then releasing in the environment. The compartment will be protected by Amifostine.

- Tumour model:

As mentioned, the aim is to highlight the advantages of using antibody as part of the Amifostine molecule, after conjugation via a linker. The Amifostine as antibody-based has the ability of reaching the target and then releasing in the environment area around the tumour (normal tissues). Amifostine doses do not need to be quantified based on the body weight, because Amifostine with this investigation approach will be directly delivered to the desire area once associated with the antibody associated. In fact, conjugated-Amifostine (*immune-radioprotector*) dose is a more suitable localizer than Amifostine dose (alone) in radiotherapy. After collecting the data (summarized in different tables - Chapter 4), we built the model based on the physiology-based equations detailed above. The differential equations were solved to give the quantity of molecule in each compartment as function of time. The rate change of the molecule concentration in the compartments is shown in figure 19. Overall uptake in each tissue has two decay clearances: first decay phase ($\alpha$) which is fast and rapidly falls dawn, which indicates an

initial clearance transport of the molecule mass in the system. The second decay phase ($\beta$) is the slow clearance of molecule from the body.

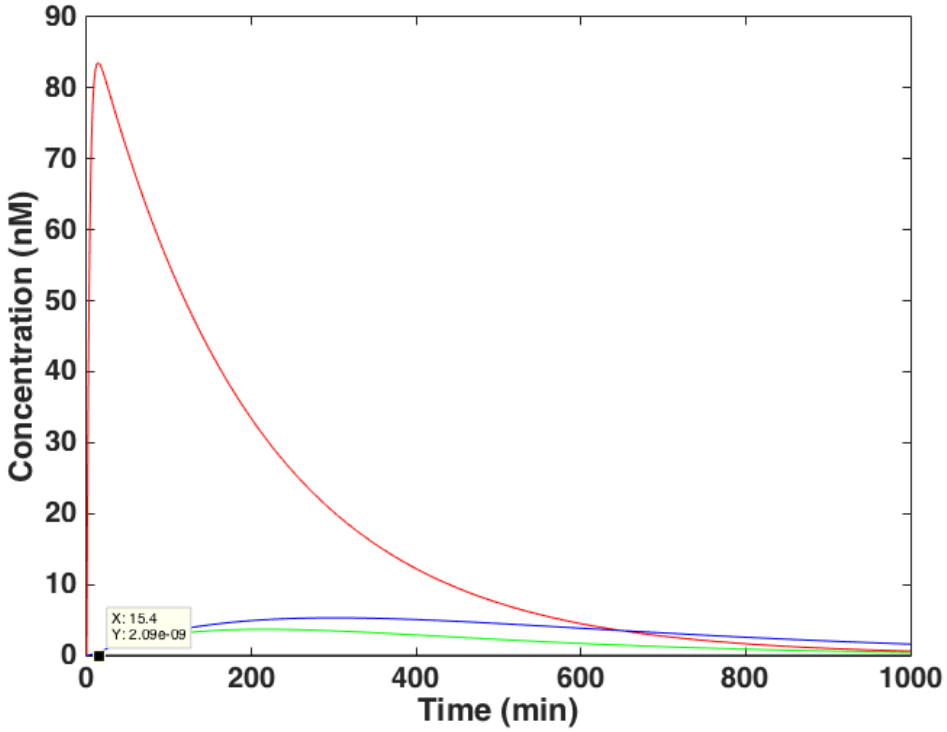


Figure 20: Full system without normalization for each compartment.

Table6-1: Data of peaks in tumour model (immuno-radioprotector system).

| | $C_{max}$ | $T_{max}$ |
|---|---|---|
| $C_{v,t}$ | 83.54 nM | 14min |
| $C_{i,t}^{f}$ | $2.09\times10^{-9}$nM | 15.4min |
| $C_{i,t}^{B}$ | 3.687 nM | 217min |
| $C_{N,t}^{f'}$ | 5.298 nM | 300.3 min |

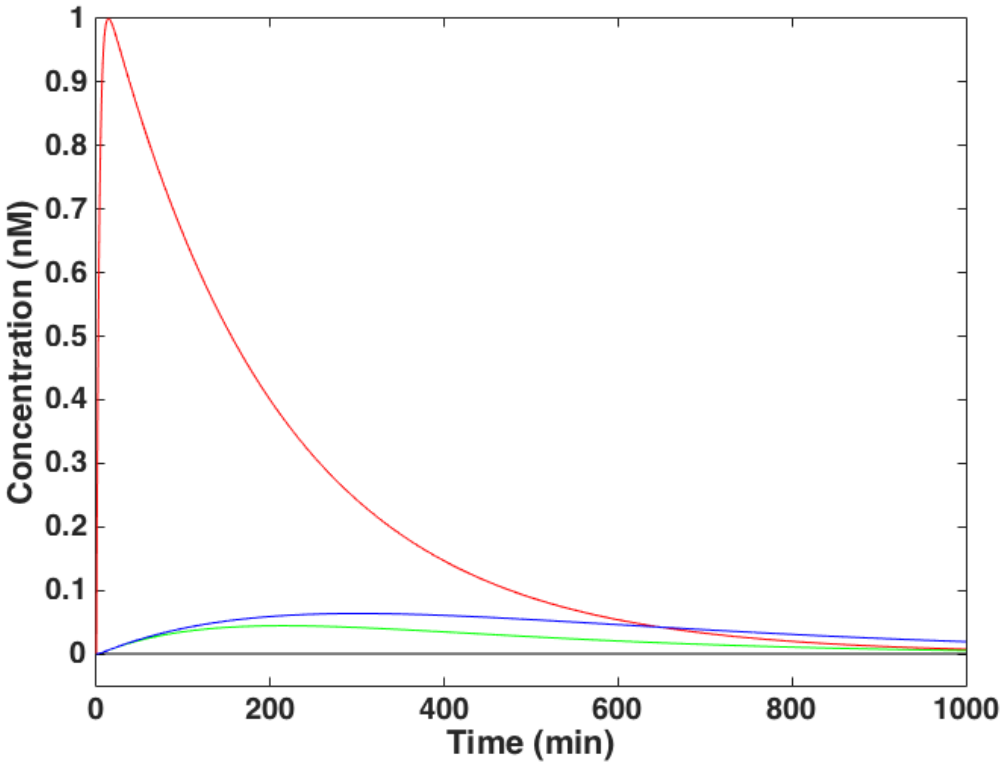


Figure 21: The rate of change of immuno-radioprotector in tumour model normalized for time respect.

The system follows the same behaviour of the reference model in vascular compartment and interstitial compartment (two sub-compartments). The red curve again overlaps the one published in [4] (vascular space – Cv). However, in the reference model, the lymph flow was set as zero because of the physiology of the model, while in our model, the elimination was taking place during the transportation of the molecule. So the system will not eliminate only from the interstitial based on the physiology of the molecule (immune-radioprotector). The molecule will be transported to the concern area of protection which is the normal tissue near by the tumour. This is the novelty/contribution of the third compartment ($C_{N,t}^{f}$) introduced by our model, where

most of the free molecule antibody-based will transport from the first sub-compartment interstitial part ( $C_{i,t}^{f}$).

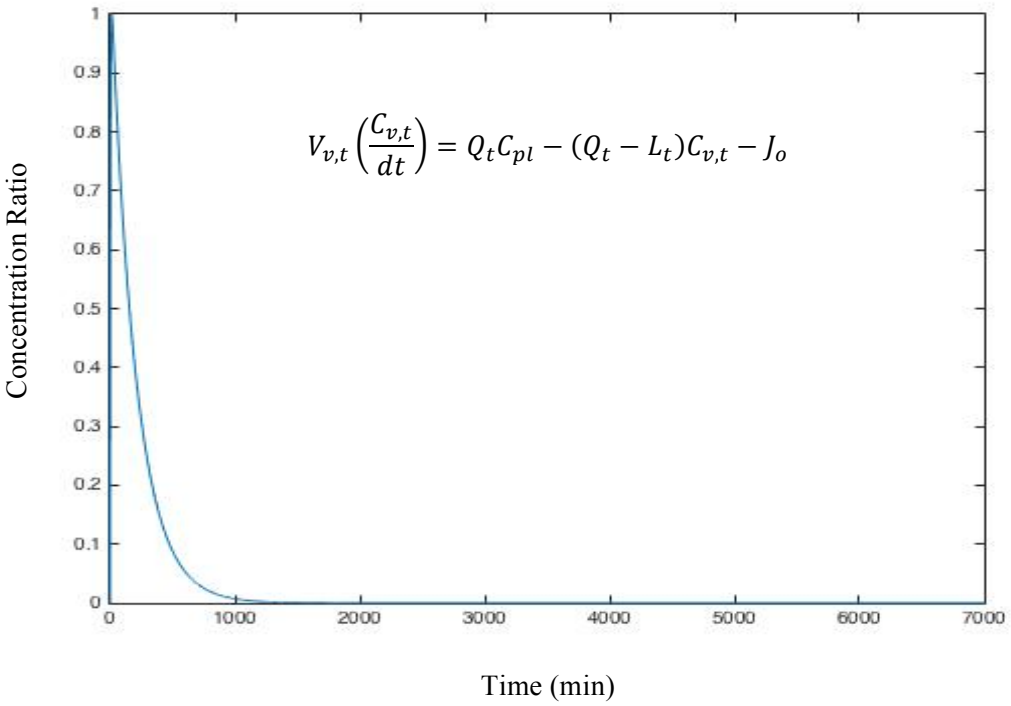


Figure 22: Normalized concentration ($\boldsymbol{C_{v,t}}$) as function of time.

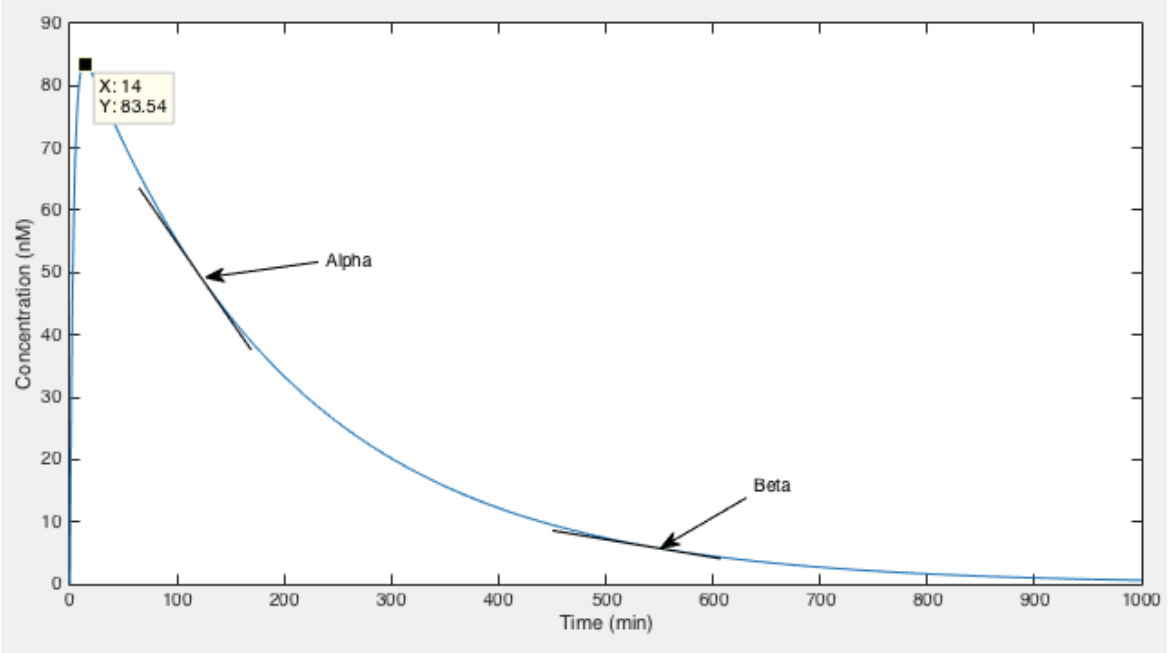


Figure 23: Vascular compartment concentration in the tumour for immuno-radioprotector.

Figures 20 and 21 show the concentration of the molecule in the vascular space. A concentration value of 83.54 nM was reached after 14 min in the targeted tissue (tumour). In tumour, the total concentration will be under two rates constant of association and disassociation between free molecule space and bound molecule space both in interstitial tissue (figures 22 and 23). Then, we can observe on figure 23 that the concentration value is very low compared with the one in other compartments of the same system, because $C_{i,t}^{f}$ is working as the momentum waiting of concentration flow in the compartment. So, the molecule is rapidly cleared from this compartment by two ways $C_{i,t}^{B}$ and/or $C_{N,t}^{f'}$.

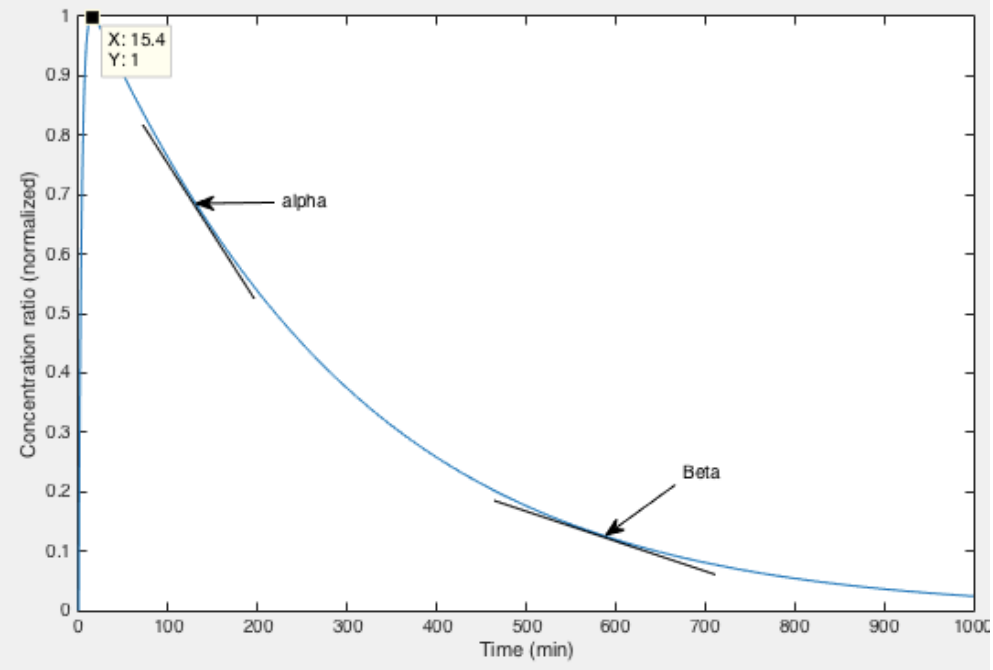


Figure 24: Concentration ratio in interstitum space for free antibody distribution ($\boldsymbol{C_{i,t}^{f}}$ (Normalized).

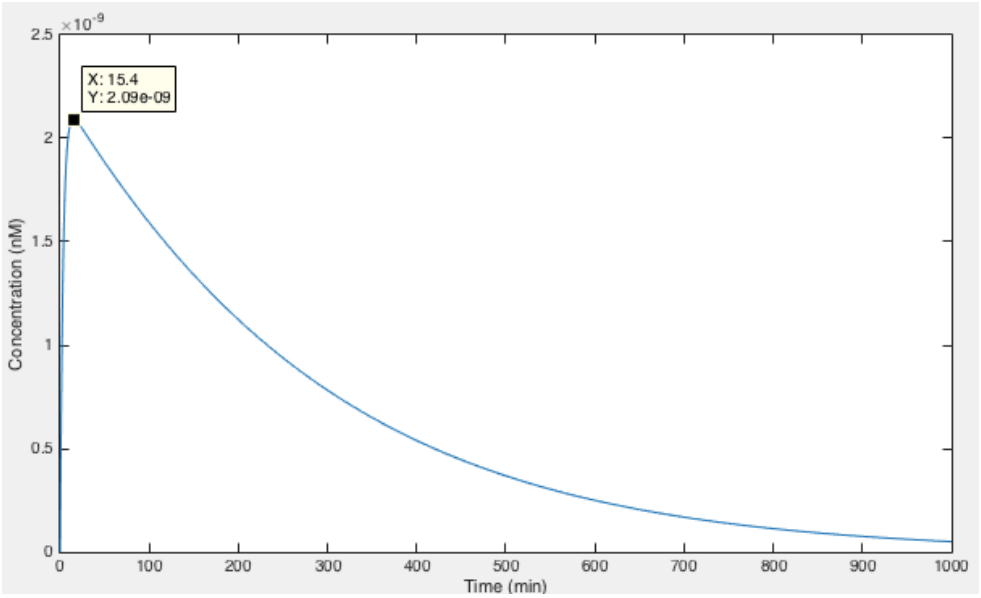


Figure 25: Free molecule (immuno-radioprotector) compartment (interstitial space$\boldsymbol{C_{i,t}^{f}}$).

The other part of interstitium compartment is for the bounding antibody concentration in this space. The bounded antibody-based molecule with Amifostine is now accumulated and then eliminated by the constant rate ($K_{e,t}$). Amifostine in this compartment will not affect the radiotherapy efficiency by protection because Amifostine will be eliminated from the tumour without making any protection on the targeted cell. Indeed, the low pH (acidic) of tumour is not suitable to active the drug (Figure 24). This figure (Figure 24) has a broad distribution in time. From the graph, there was a highlighted gap in the maximum time when we make comparing between $C_{i,t}^{B}$ and $\boldsymbol{C_{N,t}^{f'}}$. In this case, the maximum concentration of 3.687 nM is reached after 217 min. The concentration is very low comparing with the initial concentration in vascular space, which is acceptable because it will be eliminated from the compartment with no benefit in the tumour for the *immuno-radioprotector* molecule.

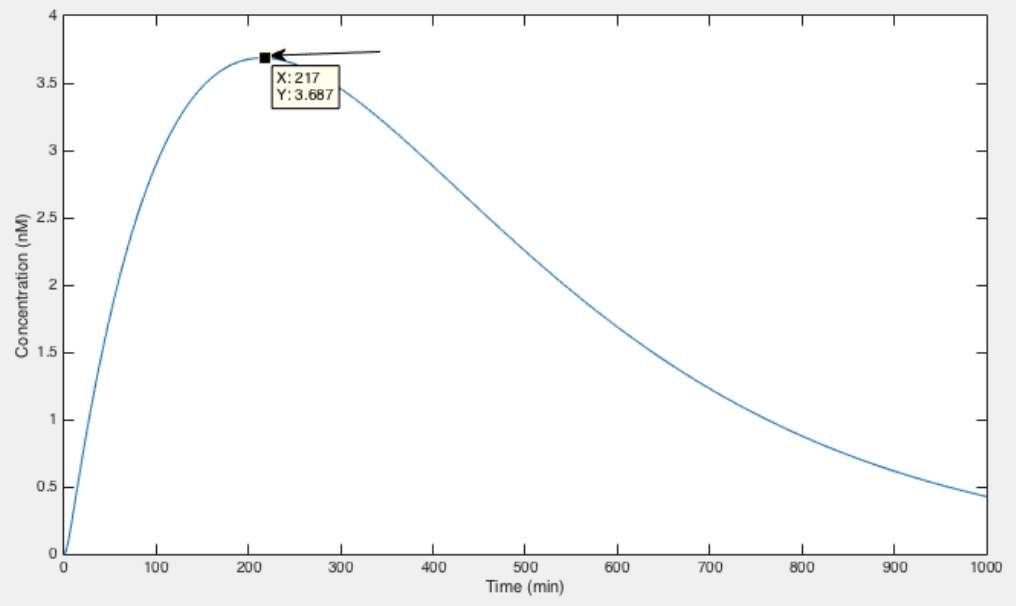


Figure 26: Bound antibody distribution in the interstitium space of tumour $\boldsymbol{C_{i,t}^{B}}$.

For the third compartment, we got the expected result. In fact, figure 25 shows a wide distribution of concentration with time. The maximum concentration value is reached in a wide time range of [200.2, 400.4] min, highlighting the stability of the concentration inside the normal tissue and the fact that it is really working. Also, comparing with the tumour compartment that already took a certain concentration (3.687 nM), the new compartment has a largest concentration in the system after the input concentration coming from the vascular space with 5.298 nM (Figures 26 and 27).

Thus, this compartment provides a suitable protection level during the radiotherapy fraction. Moreover, Amifostine will find the right environment of pH and alkaline phosphatases enzyme that will activate Amifostine to make the protection of normal tissue.

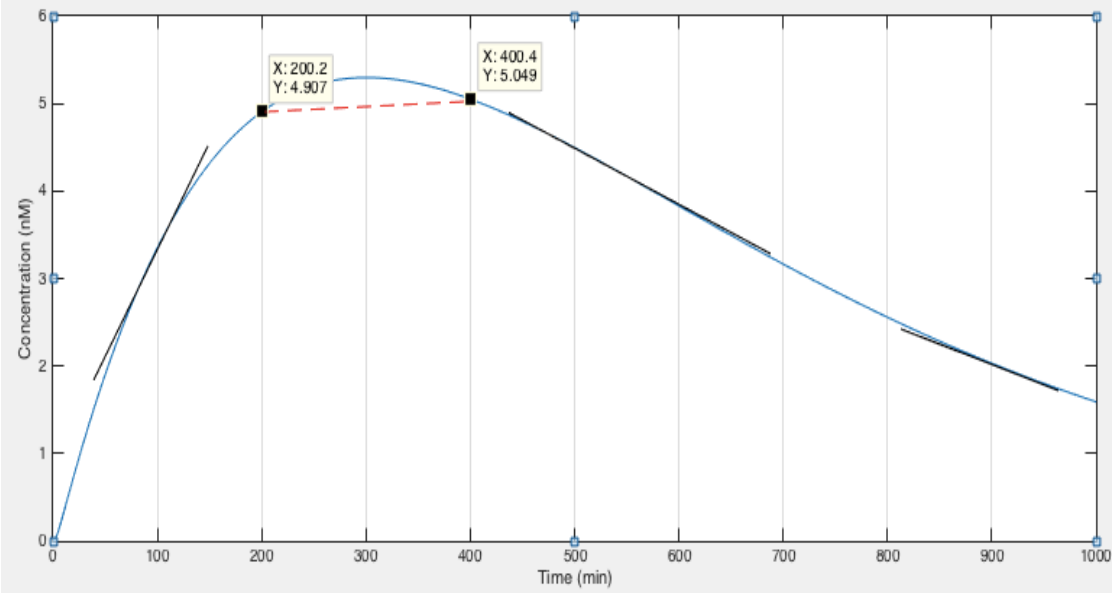


Figure 27: Concentration of immuno-radioprotector molecule in the normal tissue (protected area).

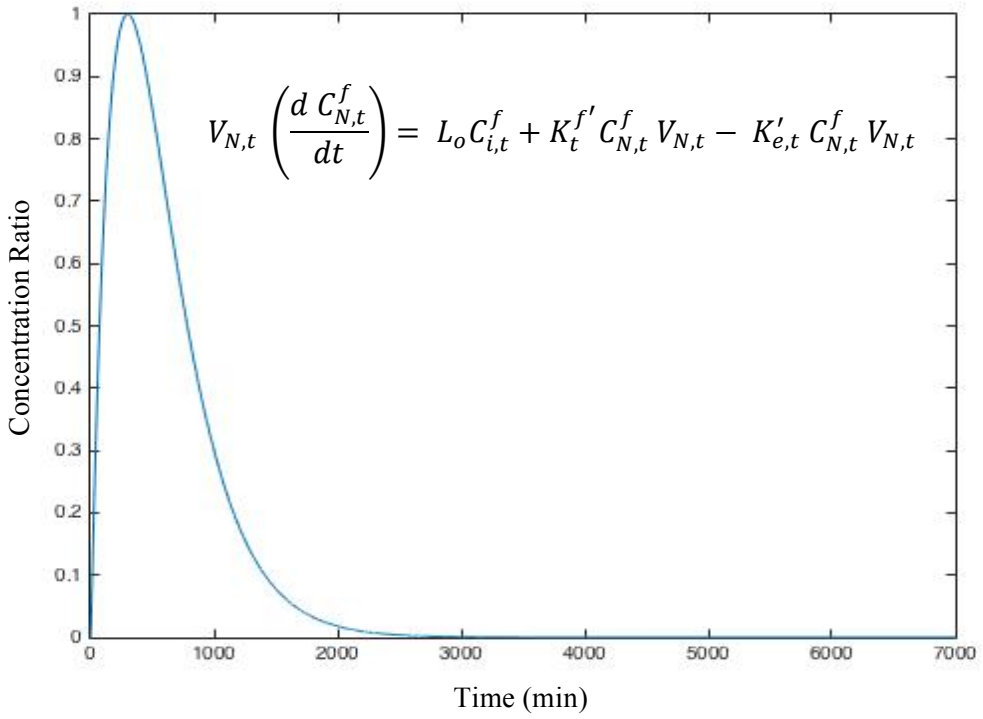


Figure 28: The concentration ratio for protection tissues around the target $\boldsymbol{C^{f'}_{N,t}}$

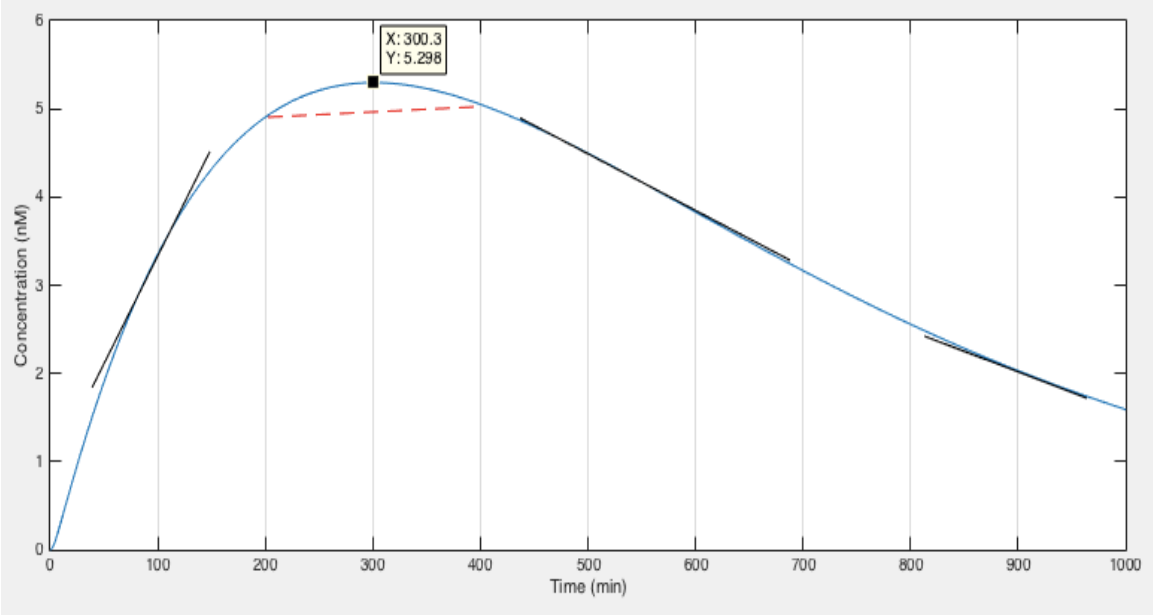


Figure 29: Maximum concentration in the normal tissue $\boldsymbol{C^{f'}_{N,t}}$.

- Liver model

The second organ in the same system is the responded organ for elimination of the molecule. Liver is related to the lymph vessels so no more bound antibody in liver as confirmed by figure 28. The vascular compartment describes the remaining amount of molecule in the system (red) while other compartment will accumulate the concentration in the liver at this point of the system. At the point (1522 min, 0.08163 nM)) both concentration ratio will be at equilibrium level of fluid flow rate (at t = 633.6 min). This means that both compartments are inversely reached each other as function of time.

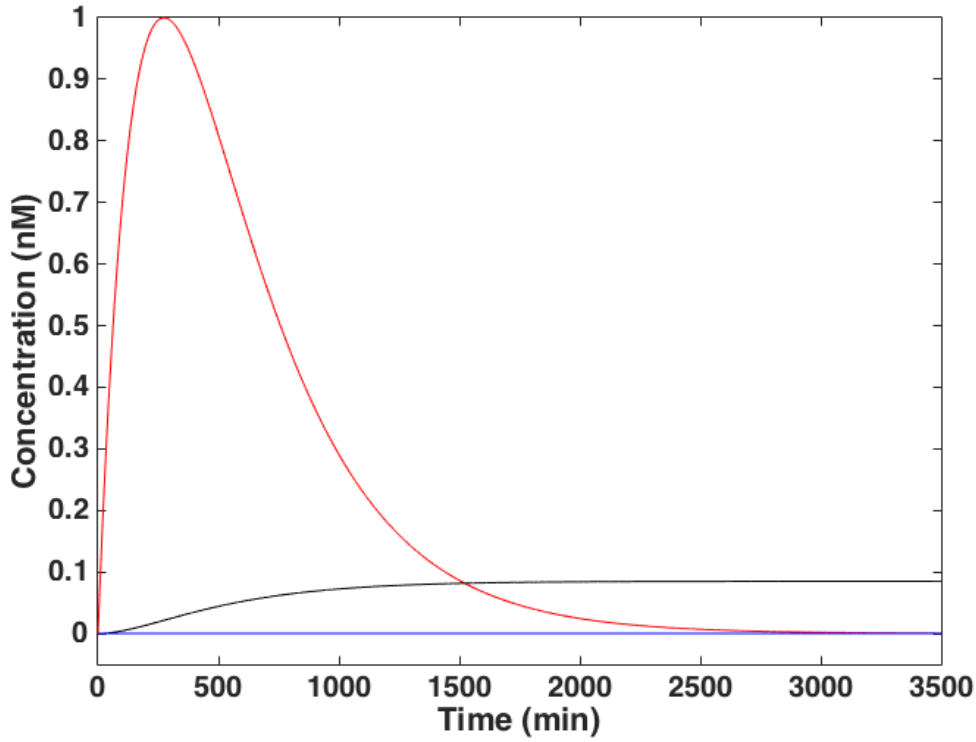


Figure 30: Liver model elimination. The red line is for the vascular concentration ratio and the blue line for the interstitial compartment.

Table 6-2: Data of peaks in liver model (immuno-radioprotector system).

| | $C_{max}$ | $T_{max}$ |
|---|---|---|
| $C_{v,t}$ | 21.7296 nM | 273.7 min |
| $C_{i,t}^{f}$ | 1.8411 nM | 2989 min |
| $C_{i,t}^{B}$ | 0 | 0 |
| $C_{N,t}^{f'}$ | 0 | 0 |

Finally, we compared our results with those given by the reference model (two-compartment model [4], stated as model (1)). Our model (model (2)) is partly a dependent-system on the reference model because the common parameters between the two systems. This is the reason why concentrations in vascular space in both systems are reaching their maximum at the same time (14min), Table 6-1.

The second compartment is for the free molecule (IgG and immune-radioprotector) in interstitium space. In this compartment, the obtained time is slightly different from the one in model (1). In fact, the reference model is reaching the maximum point before our model because there are three constant rates that can affect this sub-compartment and it is working as distribution pint to others compartment.

The third concentration in sub-compartment of interstitium space (tumour) is heading to the maximum time in model 2 faster than model (1). That gives a good explanation that the immuno-radioprotector molecule is quickly eliminated from the tumour.

Table 6-3: Data comparative value in time

| | $T_{max}$ reference model | $T_{max}$ from the proposed model |
|---|---|---|
| $C_{v,t}$ | 14 min | 14min |
| $C_{i,t}^{f}$ | 16.8 min | 15.4min |
| $C_{i,t}^{B}$ | 250.6 min | 217min |
| $C_{N,t}^{f'}$ | - | [200.2-400.4] min |

## 5.2 Effect of the initial concentration

It is useful to study how some of the parameters behave within the system and how they can influence its response. In our system most of the parameters are kinetic parameters or physiological parameters and thus, as explained previously, are not suitable for this kind of study. So we focused on the initial concentration of the system. The advantage of this analysis is to understand what it will change when we vary the input value (molecular dose) of the system. In fact, varying the input value can provide a strong evidence of curve behaviour, giving the full meaning of the relationship between the initial concentration and the concertation in each compartment.

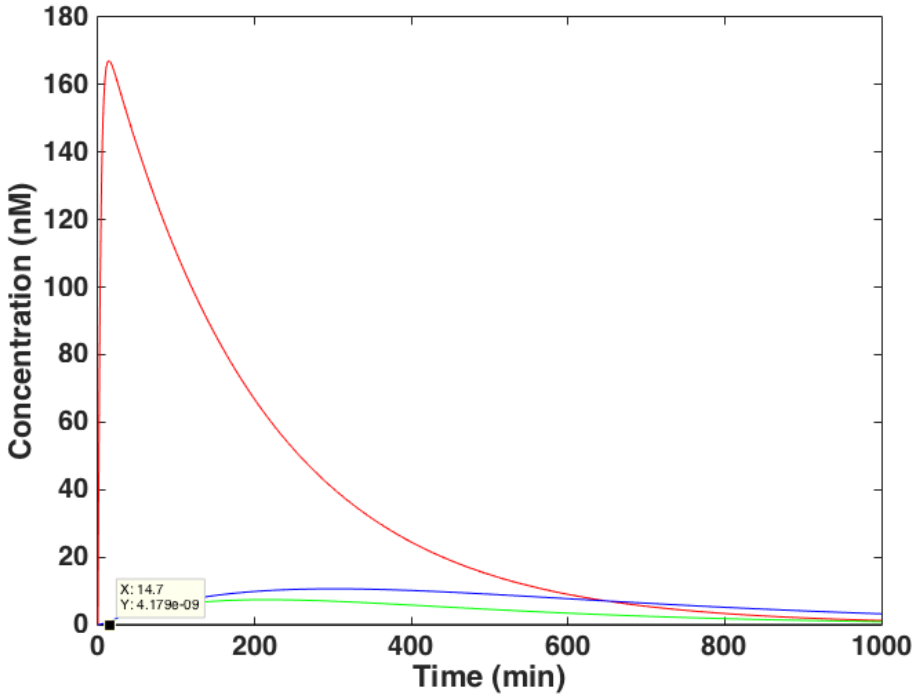


Figure 31: Full system concentration after increasing the initial concentration by a factor of 2.

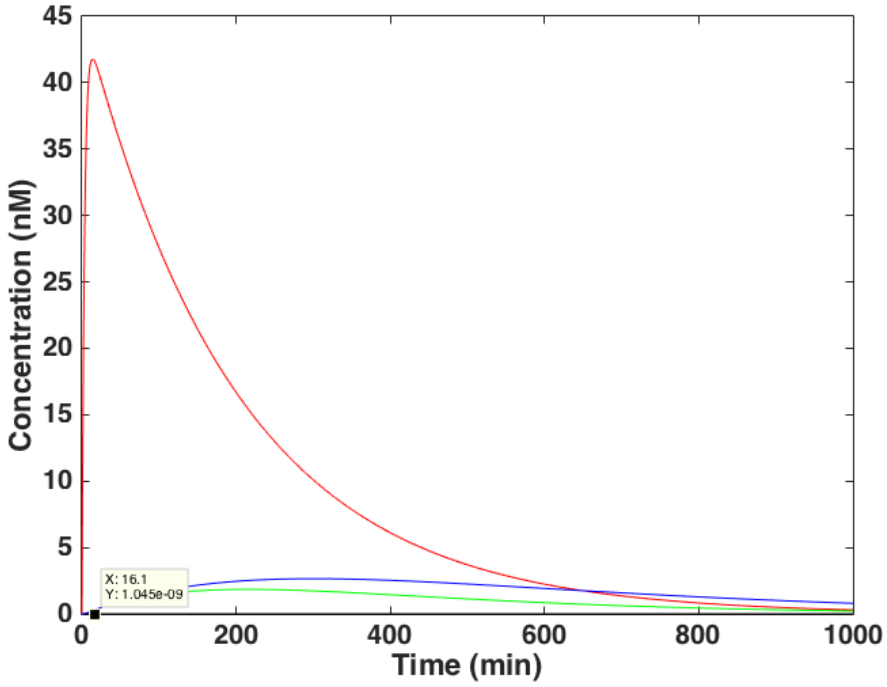


Figure 32: Full system concentration after decreasing the initial concentration by a factor of 2.

The results are summarized in Table 6-2. In this table, the first column represents the original model with initial concentration ($C_0 = \frac{1792.7\ mg}{20\ ml}$), showing the highest point concentration in each compartment. The second column represents the maximum peaks when the initial concentration is doubled ($C_0 = 2(\frac{1792.7\ mg}{20\ ml})$) and the last column is when the initial concentration is divided by a factor of 2, i.e., $C_0 = 0.5(\frac{1792.7\ mg}{20\ ml})$.

Table 6-4: The peaks of each compartment (after varying the initial concentration).

| | $C_0 = \frac{1792.7\ mg}{20\ ml}$ | $C_0 = 2\ (\frac{1792.7\ mg}{20\ ml})$ | $C_0 = 0.5\ (\frac{1792.7\ mg}{20\ ml})$ |
|---|---|---|---|
| $C_{v,t}$ | (14 min, 83.54 nM) | (14 min, 167.1 nM) | (14 min, 41.77 nM) |
| $C_{i,t}^{f}$ | (15.4 min, 2.09× $10^{-9}$nM) | (14.7 min, 4.179× $10^{-9}$nM) | (15.4 min,1.045× $10^{-9}$nM) |
| $C_{i,t}^{B}$ | (214.9 min, 3.687 nM) | (214.9 min, 7.374 nM) | (214.9 min, 1.843 nM) |
| $C_{N,t}$ | (301 min, 5.298 nM) | (301.35 min, 10.6 nM) | (300.65 min, 2.649 nM) |

## 5.3 Model limitations

Even if this work was focused on only two organs, the tumour as the desired area for releasing the molecule and the liver as the elimination zone of the drug from the system, the proposed model has the ability to be extended into a full system physiology by integrating all organs into one system. However, it suffers from a lack of real data, and therefore, cannot be efficient used by the medical staff in its current form.

This system was built based on ordinary first order equations, which can be considered as a first order approximation. Higher orders could be considered for more accuracy. However, since we used prodrug agents (amifostine), which are in an inactive form when administrated into the system, they have only one step activation and thus can be accurately modeled by first order differential equations.

## 5.4 Conclusion

In this chapter, we discussed the results obtained with the proposed three-compartment model. In the absence of real data, the pharmacokinetics study of *immuno-radioprotector* and its metabolite molecule in the normal tissues were described based on normalized graphs.

# Chapter 6. Conclusion and future work

## 6.1 Summary of work

In this project we were interested in developing a model to evaluate the effect of a radioprotector drug called amifostine. Amifostine is a protector agent that can scavenge and stop the side effect of ionizing radiation. It is the only drug has been approved for clinical use because of the benefit it provides as protection for the normal tissues during a radiotherapy session. Despite there are issues in this drug related to its high toxicity and relative cost. Conjugated amifostine with an antibody has the feature of localization when attached to a specific receptor in the body. The main contribution of this work was to propose a three pharmacokinetic compartment model to study the transportation of the molecule. Hence, we developed and simulated the system of IgG based on mathematical equations and mass balance.

*Immuno-radioprotector* molecule involves several approaches (two-pore theory and starling's theory) to deal with targeted radiotherapy and for that, we built a system based on the physiological mechanism. We decided to use an existing model as our main stone to further propose a more advanced model. We used the two-pore theory to show the molecule flow rate controlled by filtration and reflection through the microvascular walls.

The concentration in each organ (tumour and liver) will be transported from the blood to the spaces based on the pore sizes, which control this flow into and out of the organs.

## 6.2 Future work

In the absence of real data, the proposed three-compartment model used IgG antibody data as a first stage. The next stage of this work would be to implement the drug and investigate its behaviour into the organs, using real and updated clinical data.

Also, all constant rates should be studied and precisely evaluated using our model. In fact, one need to revaluate the drug parameters and determine their values based on relevant relationship parameters that control the PK model. Indeed, when the disassociation rate constant for the binding of Ab is smaller than the elimination rate constant ($K^r < K_e$) the antibody will penetrate the tumour cell (internalization). On the other hand, when ($K^r > K_e$), the antibody will dissociate prior to internalization and diffuse into the tumour. It is therefore crucial to evaluate such key parameters.

Finally, we should evaluate the average window time suitable for an antibody to deliver it to the receptor with a maximum time of association rate.

# References


[1] Andreassen, C. N., Grau, C., and Lindegaard, J. C. (2003). Chemical radioprotection: a critical review of amifostine as a cytoprotector in radiotherapy. In Seminars in radiation oncology. *WB Saunders*, (Vol. *13*, No. 1, pp. 62-72).

[2] Chari, R. V. (2007). Targeted cancer therapy: conferring specificity to cytotoxic drugs. *Accounts of chemical research,* (Vol. *41*, No. 1, pp. 98-107).

[3] Shirazi, A., Ghobadi, G., and Ghazi-Khansari, M. (2007). A radiobiological review on melatonin: a novel radioprotector. *J. of radiation research*, (Vol. *48*, No. 4, pp. 263-272).

[4] Green, A. J., Johnson, C. J., Adamson, K. L., and Begent, R. H. J. (2001). Mathematical model of antibody targeting: important parameters defined using clinical data. *Physics in medicine and biology*, (Vol. *46,* No. 6, pp. 1679–1693).

[5] Dosio, F., Brusa, P., and Cattel, L. (2011). Immunotoxins and anticancer drug conjugate assemblies: the role of the linkage between components. *Toxins*, (Vol. *3,* No. 7, pp. 848-883).

[6] Thomas J., Kremer B., Bruchhausen Y., and Rychlik R. (1999). Cost of Managing Mucositis and Xerostomia in Head and Neck Cancer Patients Undergoing Chemoradiotherapy (CRT) or Radiation (RT). *Value in Health*, (Vol. *2*, No. 3, pp. 197).

[7] Ng, K.-H. (2003). Electromagnetic Fields and Our Health; Non-Ionizing Radiations–Sources, Biological Effects, Emissions and Exposures. *Proceedings of*

*Int. Conf. on Non-Ionizing Radiation at UNITEN* (pp. 1-16). Kuala Lumpur, Malaysia: Electromagnetic Fields and Our Health.

[8] Fleet, A. (2006). Radiobiology for the Radiologist: Eric J. Hall, Amato J. Giaccia, Lippincott Williams and Wilkins Publishing; ISBN 0-7817-4151-3; 656 pages.

[9] Weiss, J. F. and Landauer, M. R. (2009). History and development of radiation-protective agents. *Int. J. of radiation biology*, (Vol. *85,* No. 7, pp. 539-573).

[10] Cadet, J., Delatour, T., Douki, T., Gasparutto, D., Pouget, J. P., Ravanat, J. L., and Sauvaigo, S. (1999). Hydroxyl radicals and DNA base damage. *Mutation Research/Fundamental and Molecular Mechanisms of Mutagenesis*, (Vol. *424,* No. 1, pp. 9-21).

[11] Pawlik, T. M., and Keyomarsi, K. (2004). Role of cell cycle in mediating sensitivity to radiotherapy. *Int. J. of Radiation Oncology – Biology - Physics*, (Vol. *59*, No. 4, pp. 928-942).

[12] Arora, R. (2008). *Herbal radiomodulators: applications in medicine, homeland defence and space*. CABI.

[13] Kelsey, C. A., Heintz, P. H., Chambers, G. D., Sandoval, D. J., Adolphi, N. L., and Paffett, K. S. (2013). *Radiation Biology of Medical Imaging*. J. Wiley & Sons.

[14] Jagetia, G. C., and Reddy, T. K. (2005). Modulation of radiation-induced alteration in the antioxidant status of mice by naringin. *Life Sciences*, (Vol. *77,* No. 7, pp. 780-794).

[15] F.A. Stewart, A.V. Akleyev, M. Hauer-Jensen, J.H. Hendry, N.J. Kleiman, T.J. MacVittie, B.M. Aleman, A.B. Edgar, K. Mabuchi, C.R. Muirhead, R.E. Shore., and W.H. Wallace. (2012). ICRP publication 118. *ICRP statement on tissue reactions and early and late effects of radiation in normal tissues and organs: threshold doses for tissue reactions in a radiation protection context*. Ottawa, Canada (Vol. 41, No. 1, pp. 1-322).

[16] Marcu, L., Bezak, E., and Allen, B. J. (2012). *Biomedical Physics in Radiotherapy for Cancer*. Csiro publishing.

[17] Koukourakis, M. I. (2002). Amifostine in clinical oncology: current use and future applications. *Anti-cancer drugs*, (Vol. *13,* No. 3, pp. 181-209).

[18] Citrin, D., Cotrim, A. P., Hyodo, F., Baum, B. J., Krishna, M. C., and Mitchell, J. B. (2010). Radioprotectors and mitigators of radiation-induced normal tissue injury. *The oncologist*, (Vol. *15*, No. 4, pp. 360-371).

[19] Nair, C. K., Parida, D. K., and Nomura, T. (2001). Radioprotectors in radiotherapy. *J. of radiation research*, (Vol. *42,* No. 1, pp. 21-37).

[20] Culy, C. R., and Spencer, C. M. (2001). Amifostine. *Drugs*, (Vol. *61,* No. 5, pp. 641-684).

[21] Kouvaris, J. R., Kouloulias, V. E., and Vlahos, L. J. (2007). Amifostine: the first selective-target and broad-spectrum radioprotector. *The oncologist*, (Vol. *12,* No. 6, pp. 738-747).

[22] Korst, A. E. C., Eeltink, C. M., Vermorken, J. B., and Van der Vijgh, W. J. F. (1997). Pharmacokinetics of amifostine and its metabolites in patients. *European J. of Cancer*, (Vol. *33,* No. 9, pp. 1425-1429).

[23] Grdina, D. J., and Sigdestad, C. P. (1989). Radiation protectors: The unexpected benefits. *Drug metabolism reviews*, (Vol. *20,* No. 1, pp. 13-42).

[24] Melis, M., Valkema, R., Krenning, E. P., and de Jong, M. (2012). Reduction of renal uptake of radiolabeled octreotate by amifostine coadministration. *J. of Nuclear Medicine*, (Vol. *53,* No. 5, pp. 749-753).

[25] Bagshawe, K. D. (1987). Antibody directed enzymes revive anti-cancer prodrugs concept. *British J. of cancer*, (Vol. *56, No.* 5, pp. 531-532).

[26] Bagshawe, K. D., Springer, C. J., Searle, F., Antoniw, P., Sharma, S. K., Melton, R. G., and Sherwood, R. F. (1988). A cytotoxic agent can be generated selectively at cancer sites. *British J. of cancer*, (Vol. *58, No.* 6, pp. 700–703).

[27] Van der Vijgh, W. J. F., and Korst, A. E. C. (1996). Amifostine (Ethyol ®): pharmacokinetic and pharmacodynamic effects in vivo. *European J. of Cancer*, (Vol. *32*, No. 4, pp. S26-S30).

[28] Bardet, E., Martin, L., Calais, G., Alfonsi, M., Feham, N. E., Tuchais, C., Boisselier, P., Dessard-Diana, B., Seng, S.H., Garaud, P., Auperin, A., and Bourhis, J. (2011). Subcutaneous compared with intravenous administration of amifostine in patients with head and neck cancer receiving radiotherapy: final

results of the GORTEC2000-02 phase III randomized trial. *J. of Clinical Oncology*, (Vol. *29,* No. 2, pp. 127-133).

[29] Lu, Z. (2007). Optimization of Amifostine Administration for Radioprotection (Unpublished doctoral dissertation). The University of Michigan, Ann Arbor, MI.

[30] Song, C. W., Griffin, R., and Park, H. J. (2006). Cancer Drug Resistance: Influence of tumor pH on therapeutic response. *In Cancer drug resistance* (pp. 21-42).

[31] Culy, C. R., and Spencer, C. M. (2001). Amifostine: An update on its clinical status as a cytoprotectant in patients with cancer receiving chemotherapy or radiotherapy and its potential therapeutic application in myelodysplastic syndrome. *Drugs*, (Vol. *61,* No. 5, pp. 641-684).

[32] Korst, A. E., Gall, H. E., Vermorken, J. B., and van der Vijgh, W. J. (1996). Pharmacokinetics of amifostine and its metabolites in the plasma and ascites of a cancer patient. *Cancer chemotherapy and pharmacology*, (Vol. *39,* No*,* 1-2, pp. 162-166).

[33] Zhou, H., and Mascelli, M. A. (2011). Mechanisms of monoclonal antibody-drug interactions. *Annual review of pharmacology and toxicology*, (Vol. *51*, pp. 359-372).

[34] Bischoff, K. B., Dedrick, R. L., Zaharko, D. S., and Longstreth, J. A. (1971). Methotrexate pharmacokinetics. *J. of pharmaceutical sciences*, (Vol. *60,* No. 8, pp. 1128-1133).

[35] Wang, W., Wang, E. Q., and Balthasar, J. P. (2008). Monoclonal antibody pharmacokinetics and pharmacodynamics. *Clinical Pharmacology and Therapeutics*, (Vol. *84,* No*,* 5, pp. 548-558).

[36] Lobo, E. D., Hansen, R. J., and Balthasar, J. P. (2004). Antibody pharmacokinetics and pharmacodynamics. *J. of pharmaceutical sciences*,(Vol. *93,* No. 11, pp. 2645-2668).

[37] Deng, R., Jin, F., Prabhu, S., and Iyer, S. (2011). Monoclonal antibodies: what are the pharmacokinetic and pharmacodynamic considerations for drug development?. *Expert opinion on drug metabolism and toxicology*, (Vol. *8,* No. 2, pp. 141-160).

[38] Rippe, B., and Haraldsson, B. (1994). Transport of macromolecules across microvascular walls: the two-pore theory. *Physiological reviews*, (Vol. *74,* No. 1, pp. 163-220).

[39] Thurber, G. M., Schmidt, M. M., and Wittrup, K. D. (2008). Antibody tumor penetration: transport opposed by systemic and antigen-mediated clearance.*Advanced drug delivery reviews*, (Vol. *60*, No. 12, pp. 1421-1434).

[40] Preziosi, L. (Ed.). (2003). *Cancer modelling and simulation*. Florida, FL, CRC Press.

[41] Stachowska-Pietka, J., Waniewski, J., Flessner, M. F., and Lindholm, B. (2006). A distributed model of bidirectional protein transport during peritoneal fluid

absorption. In *Advances in peritoneal dialysis. Conf. on Peritoneal Dialysis* (Vol. *23*, pp. 23-27).

[42] Jain, R. K. (1990). Physiological barriers to delivery of monoclonal antibodies and other macromolecules in tumors. *Cancer research*, (Vol. *50, No.* 3, pp. 814s-819s).

[43] Korthuis, R. J. (2011). Microvascular Fluid and Solute Exchange in Skeletal Muscle. Skeletal Muscle Circulation (pp. 53-66). Korthuis, R.J., and San, R., (CA). NJ: Morgan and Claypool Life Sciences.

[44] Öberg, C. M., and Rippe, B. (2014). A distributed two-pore model: theoretical implications and practical application to the glomerular sieving of Ficoll. *American J. of Physiology-Renal Physiology*, (Vol. *306,* No. 8, pp. F844-F854).

[45] Korthuis, R. J. (2011). Skeletal muscle circulation. In *Colloquium Series on Integrated Systems Physiology: From Molecule to Function* (Vol. *3*, No. 4, pp. 1-144). Morgan and Claypool Life Sciences.

[46] Baxter, L. T., Zhu, H., Mackensen, D. G., and Jain, R. K. (1994). Physiologically based pharmacokinetic model for specific and nonspecific monoclonal antibodies and fragments in normal tissues and human tumor xenografts in nude mice. *Cancer research*, (Vol. *54,* No. 6, pp. 1517-1528).

[47] Levick, J. R., and Michel, C. C. (2010). Microvascular fluid exchange and the revised Starling principle. *Cardiovascular research*, (Vol. *87*, No. 2, pp. 198-210).

[48] Scallan, J., Huxley, V. H., and Korthuis, R. J. (2010, February). Capillary fluid exchange: regulation, functions, and pathology. In *Colloquium Lectures on Integrated Systems Physiology-\ nl\ hspace* 18pt From Molecules to Function,* (Vol. *2*, No. 1, pp. 1-94). Morgan and Claypool Publishers.

[49] Mould, D. R., and Sweeney, K. R. (2007). The pharmacokinetics and pharmacodynamics of monoclonal antibodies-mechanistic modeling applied to drug development. *Current Opinion in Drug Discovery and Development*, (Vol. *10,* No. 1, pp. 84-96).

[50] Heiskanen, T., Heiskanen, T., and Kairemo, K. (2009). Development of a PBPK model for monoclonal antibodies and simulation of human and mice PBPK of a radiolabelled monoclonal antibody. *Current pharmaceutical design*, (Vol. *15*, No. 9, pp. 988-1007).

[51] Baxter, L. T., and Jain, R. K. (1996). Pharmacokinetic analysis of the microscopic distribution of enzyme-conjugated antibodies and prodrugs: comparison with experimental data. *British J. of cancer*, (Vol. *73,* No. 4, pp. 447-456).

[52] Khalil, F., and Läer, S. (2011). Physiologically based pharmacokinetic modeling: methodology, applications, and limitations with a focus on its role in pediatric drug development. *BioMed Research Int.*, (Vol. *2011,* No. 4, pp. 1-13).

[53] Coddington, E. A., and Carlson, R. (1997). Linear ordinary differential equations. Philadelphia, PA: *Society for Industrial and Applied Mathematics*.

[54] Sepp, A., Berges, A., Sanderson, A., and Meno-Tetang, G. (2015). Development of a physiologically based pharmacokinetic model for a domain antibody in mice using the two-pore theory. *J. of pharmacokinetics and pharmacodynamics*, (Vol. *42,* No. 2, pp. 97-109).

[55] Baxter, L. T., Zhu, H., Mackensen, D. G., Butler, W. F., and Jain, R. K. (1995). Biodistribution of monoclonal antibodies: scale-up from mouse to human using a physiologically based pharmacokinetic model. *Cancer research*, (Vol. *55,* No. 20, pp. 4611-4622).

[56] Wei, J. (1994). *Advances in Chemical Engineering*. London: Academic Press. (Vol. *19*, pp. 1-425).

[57] Halls. (2015). *Body Surface Area*. Retrieved from Halls: http://halls.md/body-surface-area/bsa.htm, Last access July 6, 2015.

[58] Walker, D. M., Walker, V. E., and Poirier, M. C. (2007). *Patents*. Retrieved from Google: http://google.com/patents/WO2007123868A2?cl=en, Last access July 6, 2015.

[59] Ferl, G. Z., Wu, A. M., and DiStefano III, J. J. (2005). A predictive model of therapeutic monoclonal antibody dynamics and regulation by the neonatal Fc receptor (FcRn). *Annals of biomedical engineering*, (Vol. *33,* No. 11, pp. 1640-1652).